Harmonization and Annotation of Single-cell Transcriptomics data with Deep Generative Models

Chenling Xu[*,1], Romain Lopez[*,2], Edouard Mehlman[*,2,3],
Jeffrey Regier[2], Michael I. Jordan[2,4] & Nir Yosef[†,1,2,5,6]

[1]Center for Computational Biology
University of California, Berkeley

[2]Department of Electrical Engineering and Computer Sciences
University of California, Berkeley

[3]Centre de Mathématiques Appliquées
Ecole polytechnique, Palaiseau

[4]Department of Statistics
University of California, Berkeley

[5]Ragon Institute of MGH, MIT and Harvard

[6]Chan-Zuckerberg Biohub Investigator

[*] These authors contributed equally to this work.

[†] Corresponding author. Email: niryosef@berkeley.edu (N.Y.).

Abstract

As single-cell transcriptomics becomes a mainstream technology, the natural next step is to integrate the accumulating data in order to achieve a common ontology of cell types and states. However, owing to various nuisance factors of variation, it is not straightforward how to compare gene expression levels across data sets and how to automatically assign cell type labels in a new data set based on existing annotations. In this manuscript, we demonstrate that our previously developed method, scVI, provides an effective and fully probabilistic approach for joint representation and analysis of cohorts of single-cell RNA-seq data sets, while accounting for uncertainty caused by biological and measurement noise. We also introduce single-cell ANnotation using Variational Inference (scANVI), a semi-supervised variant of scVI designed to leverage any available cell state annotations — for instance when only one data set in a cohort is annotated, or when only a few cells in a single data set can be labeled using marker genes. We demonstrate that scVI and scANVI compare favorably to the existing methods for data integration and cell state annotation in terms of accuracy, scalability, and adaptability to challenging settings such as a hierarchical structure of cell state labels. We further show that different from existing methods, scVI and scANVI represent the integrated datasets with a single generative model that can be directly used for any probabilistic decision making task, using differential expression as our case study. scVI and scANVI are available as open source software and can be readily used to facilitate cell state annotation and help ensure consistency and reproducibility across studies.

Introduction

Recent technological improvements in microfluidics and low volume sample handling [1] have enabled the emergence of single-cell transcriptomics [2, 3] as a popular tool for analyzing biological systems [4, 5, 6]. This growing popularity along with a continued increase in the scale of the respective assays [7] has resulted in massive amounts of publicly available data and motivated large scale community efforts such as the Human Cell Atlas [8], Tabula Muris [9] and the BRAIN Initiative Cell Census Network [10]. The next natural step in the evolution of this field is therefore to integrate many available datasets from related tissues or disease models in order to increase statistical robustness [11], achieve consistency and reproducibility among studies [12, 13], and ultimately converge to a common ontology of cell states and types [8, 14].

A fundamental step toward the ideal of a common ontology is data *harmonization*, namely integration of two or more transcriptomics datasets into a single dataset on which any downstream analysis can be applied. We use the term harmonization rather than *batch effect correction* in order to emphasize that the input datasets may come from very different sources (*e.g.*, technology, laboratory), and from samples with a different composition of cell types. A wide range of methods have already been developed for this fundamental problem, initially for Microarrays and later on for bulk RNA sequencing, such as ComBat [15] and limma [16] which rely on generalized linear models with empirical Bayes shrinkage to avoid over-correction. More recently, similar methods have been proposed specifically for single-cell RNA sequencing (scRNA-seq), such as ZINB-WaVE [17], which explicitly accounts for the overabundance of zero entries in the data. However, because of their linear assumptions, these approaches may not be appropriate when provided with a heterogeneous sample that includes different cell states, each of which may be associated with a different sample-to-sample bias [12]. With these limitations in mind, the next generation of methods turned to non-linear strategies. Broadly speaking, each of these methods includes a combination of two components: (i) joint factorization of the input matrices (each corresponding to a different dataset) to learn a joint low-dimensional latent representation. This is usually done with well established numerical methods, such as integrative non-negative matrix factorization (LIGER [18]), singular value decomposition (Scanorama [19]), or canonical correlation analysis (Seurat Alignment [13]); (ii) additional non-linear transformation of the resulting latent representations so as to optimally "align" them onto each other. This is usually done using heuristics, such as alignment of mutual nearest neighbors (MNN [12], Scanorama [19] and Seurat Anchors [20]), dynamic time warping (Seurat Alignment [13]) or quantile normalization (LIGER [18]). While this family of methods has been shown to effectively overlay different datasets, it suffers from two important limitations. First, an explicit alignment procedure may be difficult to tune in a principled manner and consequently result in over-normalization, especially in challenging cases where the cell type composition is different between datasets and when technical differences between samples are confounded with biological differences of interest. Second, the alignment is done in an ad hoc manner and lacks probabilistic interpretability. Consequently, the resulting harmonized dataset is of limited use and cannot be directly applied for differential expression and other probabilistic decision-making tasks.

Another recent line of work makes use of neural networks to learn a joint representation of multiple datasets (SAUCIE [21]) or project one dataset into another (maximum mean discrepancy [MMD] ResNet [22]). These methods rely on an explicit non-parametric measure of discrepancy between probability distributions (MMD) to match either the latent spaces or directly the gene expression values from pairs of datasets. However, using the MMD with a universal kernel explicitly assumes that the cell type proportion is similar in all the datasets, which may be less suitable in the general case of data harmonization.

Besides harmonization, another important and highly related problem is that of automated *annotation* of cell state. In principle, there are two ways to approach this problem. The first is *ab initio* labeling of cells based on marker genes or gene signatures [13, 23, 24]. While this approach is intuitive and straightforward, its performance may be affected in the plausible case where marker genes are absent due to limitations in sensitivity. The second approach is to "transfer" annotations between datasets. In the simplest scenario, we have access to one dataset where states have been annotated either *ab initio*, or using additional experimental measurements (e.g., protein expression [3, 25] or lineage tracing [26]) and another, unannotated dataset from a similar condition or tissue. The goal is to use the labeled data to derive similar annotations for the second dataset, whenever applicable. This task is often complicated by factors such as

differences in technology (e.g., using Smart-Seq2 data to annotate 10x Chromium data), partial overlap in cell type composition (i.e., not all labels should be transferred and not all unannotated cells should be assigned a label), complex organization of the labels (e.g., hierarchy of cell types and sub-types [27], continuum along phenotypic or temporal gradients), partial labeling (i.e., only a subset of cells from the "annotated" dataset can be assigned a label confidently), and the need to handle multiple (more than 2) datasets in a principled and scalable manner. One way to address the annotation problem with this approach is learning a classifier [27, 28] in order to predict a fixed stratification of cells. Another, more flexible approach is to transfer annotations by first harmonizing the annotated and unannotated datasets, thus also gaining from the benefits of having a single dataset that can be subject to additional, joint, downstream analysis.

In this paper, we propose a strategy to address several of the outstanding hurdles in both of the harmonization and annotation problems. We first demonstrate that single-cell Variational Inference (scVI) [29] a deep generative model we previously developed for probabilistic representation of scRNA-seq data — performs well in both harmonization and harmonization-based annotation, going beyond its previously demonstrated capacity to correct batch effects. We then introduce single-cell ANnotation using Variational Inference (scANVI), a new method that extends scVI and provides a principled way to address the annotation problem probabilistically while leveraging any available label information. scANVI uses a semi-supervised generative model, which can be utilized for both approaches to the annotation problem. In the first scenario, we are concerned with a single dataset in which only a subset of cells can be confidently labeled (e.g., based on expression of marker genes) and annotations should then be transferred to other cells, when applicable. In the second scenario, annotated datasets are harmonized with unannotated datasets and then used to assign labels to the unannotated cells.

The inference procedure for both of the scVI and scANVI models relies on neural networks, stochastic optimization and variational inference [30, 31] and scales to large numbers of cells and datasets. Furthermore, both methods provide a complete probabilistic representation of the data, which non-linearly controls not only for sample-to-sample bias but also for other technical factors of variation such as over-dispersion, library size discrepancies and zero-inflation. As such, each method provides a single probabilistic model that underlies the harmonized gene expression values (and the cell annotations, for scANVI), and can be used for any type of downstream hypotheses testing. We demonstrate the latter point through a differential expression analysis on harmonized data. Furthermore, through a comprehensive analysis of performance in various aspects of the harmonization and annotation problems and in various scenarios, we demonstrate that scVI and scANVI compare favorably to current state-of-the-art methods.

Results

In the following we demonstrate that our framework compares favorably to the existing state of the art in the harmonization and annotation problems in terms of accuracy, scalability, and adaptability to various settings. The first part of the paper focuses on the harmonization problem and covers a range of scenarios, including harmonization of datasets with varying levels of biological overlap, handling cases where the data is governed by a continuous (e.g., pseudotime) rather than discrete (cell types) form of variation, and processing multiple (> 20) datasets. While we demonstrate that scVI performs well in these scenarios, we also demonstrate that the latent space leaned by scANVI provides a proper harmonized representation of the input datasets — a property necessary for guaranteeing its performance in the annotation problem. In the second part of this manuscript we turn to the annotation problem and study its two main settings, namely transferring labels between datasets and *ab-inito* labeling. In the first setting we consider the cases of datasets with a complete or partial biological overlap and use both experimentally- and computationally- derived labels to evaluate our performance. In the second settings, we demonstrate how scANVI can be used effectively to annotate a single dataset by propagating high confidence seed labels (based on marker genes) and by leveraging a hierarchical structure of cell state annotations. Finally, we demonstrate that the generative models inferred by scANVI and scVI can be directly applied for hypotheses testing, using differential expression as a case study.
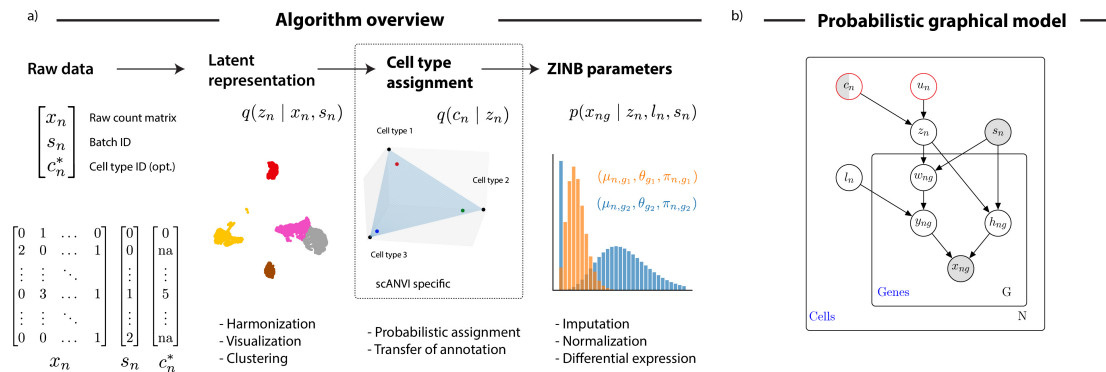
Joint modeling of scRNA-seq datasets

We consider K different scRNA-seq datasets (**Figure 1a**). A dataset indexed by $k \in \{1, \cdots, K\}$ consists of a $N_k \times G_k$ matrix where each entry records the number of transcripts observed for each of G_k genes in each of N_k cells. In this work, we use a standard heuristic to filter the genes and generate a common (possibly large) gene set of size G (**Online Methods**), and thus format our data as a unique $(\sum_k N_k) \times G$ matrix whose individual entries are noted x_{ng} — namely the expression of gene g in cell n. We use $s_n \in \{1, \cdots, K\}$ to represent the dataset from which each cell n was generated. Furthermore, a subset of the cells may be associated with a cell state annotation c_n, which can describe either discrete cell types or hierarchical cell types. More complex structures over labels such as gradients are left as a future research direction.

Since the problem of data harmonization of single-cell transcriptomics is difficult and can potentially lead to over-correction (**Figure 1b**) [32], we propose a fully-generative method as a robust and principled approach to address it. In our previous work [29], we built single-cell Variational Inference (scVI), a deep generative model where the expression level x_{ng} is zero-inflated negative binomial (ZINB) when conditioned on the dataset identifier (s_n), and two additional latent random variables. The first, which we denote by l_n, is a one-dimensional Gaussian accounting for the variation in capture efficiency and sequencing depth. The second is z_n is a low dimensional Gaussian vector that represents the remaining variability (**Figure 1c**). This vector is expected to reflect biological differences between cells, and can be effectively used for visualization, clustering, pseudotime inference and other tasks. Since the scVI model explicitly conditions on the dataset identifier, it provides an effective way of controlling for technical sample-to-sample variability. However, scVI is unsupervised and does not make use of the available annotations c_n, which can further guide the inference of an informative latent representation z_n. To this end, we present a more refined hierarchical structure for z_n. We draw z_n as a mixture conditioned on the cell annotation c_n and another latent variable u_n, accounting for further biological variability within a cell type (**Figure 1d**, **Online Methods**). We name the resulting approach single-cell ANnotation using Variational Inference (scANVI).

The variables z_n, inferred either with scVI or scANVI, provide an embedding of all cells in a single, joint latent space. Since this latent space is inferred while controlling for the dataset of origin (s_n), it inherently provides a way to address the harmonization problem. The annotation of unlabeled cells can therefore be conducted with scVI using their proximity to annotated cells in the joint latent space (e.g., using majority vote over the k-nearest neighbors). The scANVI model provides a more principled way to annotate cells, namely through a Bayesian semi-supervised approach. Once fitted, the model is able to provide posterior estimates for the unobserved cell state c_n, which can be particularly useful when labels cannot be entirely trusted. Because the marginal distribution $p(x_{ng}, c_n \mid s_n)$ if c_n observed (resp. $p(x_{ng} \mid s_n)$ otherwise) is not amenable to exact Bayesian computation, we use variational inference parameterized by neural networks to approximate it [30] (**Online Methods**).

Notably, scANVI and scVI both have a certain number of hyperparameters. In the following evaluations, conducted on different datasets and different scenarios, we use the exact same set of hyperparameters in order to demonstrate that our methods can be applied with a minimal requirement of hyperparameter tuning (**Online Methods**). We provide a robustness study for hyperparameters in the context of harmonization in **Supplementary Figure 1**. We further discuss the underlying assumptions of our framework in the context of competing harmonization methods in **Supplementary Note 1**.
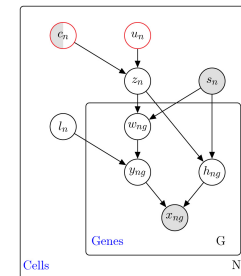
Figure 1: Harmonization of scRNA-seq datasets with generative models. (a) Schematic diagram of the variational inference procedure in both of the scVI and scANVI models. We show the order in which random variables in the generative model are sampled and how these variables can be used to derive biological insights. (b) The graphical models of scVI and scANVI. Vertices with black edges represent variables in both scVI and scANVI, and vertices with red edges are unique to scANVI. Shaded vertices represent observed random variables. Semi-shaded vertices represent variables that can be either observed or random. Empty vertices represent latent random variables. Edges signify conditional dependency. Rectangles ("plates") represent independent replication. The complete model specification and definition of internal variables is provided in the **Online Methods**
.

Datasets

We apply our method on datasets generated by a range of technologies (10x Chromium [3, 33], plate-based Smart-Seq2 [34], Fluidigm C1 [35], MARS-Seq [36], inDrop [37] and CEL-Seq2 [38]), spanning different numbers of cells (from a few thousand to over a hundred thousand cells), and originating from various tissues (mouse bone marrow, human peripheral mononuclear blood cells [PBMCs], human pancreas, mouse brain). Datasets are listed and referenced in **Supplementary Table 1**.

Harmonizing pairs of datasets with a discrete population structure

We conducted a comparative study of harmonization algorithms on four different instances, each consisting of a pair of datasets. The first pair (PBMC-CITE [25], PBMC-8K [33]) represents the simplest case, in which the two datasets come from very similar biological settings (i.e., PBMCs) and are generated by the same technology (i.e., 10x) but in different labs (i.e., akin to batch correction). A second scenario is that of similar tissue but different technologies, which we expect to be more challenging as each technology comes with its own characteristics and biases [39]. For instance, some methods (10x, CEL-Seq2) profile the end of the transcript and use Unique Molecular Identifier (UMI) to mitigate inflation in counting, whereas others (e.g., most applications of Smart-Seq2) consider the full length of the transcript without controlling for this potential bias. Additionally, some protocols (e.g., Smart-Seq2) tend to have higher sensitivity and capture more genes per cell compared to others. Finally, studies using droplet based protocols tend to produce much larger numbers of cells compared to plate-based methods. We explore three such cases, including a bone marrow 10x and Smart-Seq2 pair from the Tabula Muris project (MarrowTM-10x, MarrowTM-ss2 [9]), a pancreas inDrop and CEL-Seq2 pair (Pancreas-InDrop, Pancreas-CEL-Seq2 [40]), and a dentate gyrus 10x and Fluidigm C1 pair (DentateGyrus-10x, DentateGyrus-C1 [41]).

Successful harmonization should satisfy two somewhat opposing criteria (**Supplementary Figure 2**). On the one hand, cells from the different datasets should be well mixed; namely, the set of k-nearest neighbors (kNN) around any given cell (computed e.g., using euclidean distance in the harmonized latent space) should be balanced across the different datasets. For a fixed value of k, this property can be evaluated using the entropy of batch mixing [12], which is akin to evaluating a simple k-nearest neighbors classifier for the batch identifier (**Online Methods**). While this property is important, it is not sufficient, since it can be achieved by simply randomizing the data. Therefore, in our evaluations we also consider the extent to which the harmonized data retains the original structure observed at each dataset in isolation. Here, we expect that the set of k-nearest neighbors of any given cell in its original dataset should remain sufficiently close to that cell after harmonization. This property can be evaluated using a measure we call k-nearest neighbors purity (**Online Methods**). Clearly, this criterion can be simply optimized by not changing the input datasets, which will result in poor performance with respect to our first measure. Our evaluation therefore relies on both of these measures.

Since our results depend on the neighborhood size k, we consider a range of values - from a high resolution ($k = 10$) to a coarse ($k = 500$) view of the data. We compare scVI to several methods, including MNN [12], Seurat Alignment [13], ComBat [15] and principal component analysis (PCA). For each algorithm and pair of datasets, we report embeddings computed via a Uniform Manifold Approximation and Projection (UMAP) [42] (**Figure 2a, Supplementary Figure 3 - 6**) as well as the two evaluation metrics (**Figure 2b-c**). Overall, we observed that scVI performs well in terms of mixing, while comparing favorably to the other methods in terms of retainment of the original structure, for a wide range of neighborhood sizes and across all dataset pairs. As an example, consider the results of applying scVI and Seurat Alignment to the Tabula Muris bone marrow datasets (**Figure 2a**). As can be observed from both the entropy of batch mixing values and the visualization of the harmonized data, both methods perform well when it comes to mixing the input datasets. However, we observe that scVI performs better in retaining the original, continuous, structure of the data. Indeed, using cell type labels provided by the original publication [9], we observe that scVI captures the continuous process of myeloid cell development (from hematopoietic precursors to erythrocytes and monocytes) well, while Seurat Alignment groups the two trajectories (erythrocytes and monocytes) into separate clusters.

While scANVI was designed for the problem of cell state annotation, we also wanted to evaluate its ability to harmonize datasets, which can be seen as a prerequisite. To evaluate this,

we consider each dataset pair twice, each time using labels from one of the datasets (exploiting the semi-supervision framework of scANVI). Reassuringly, we found that scANVI is capable of effectively harmonizing the datasets, with a similar performance to that of scVI in terms of entropy of batch mixing and k-nearest neighbors purity (**Figure 2b-c**). We further explore the performance of scANVI in the annotation problem in the subsequent sections.
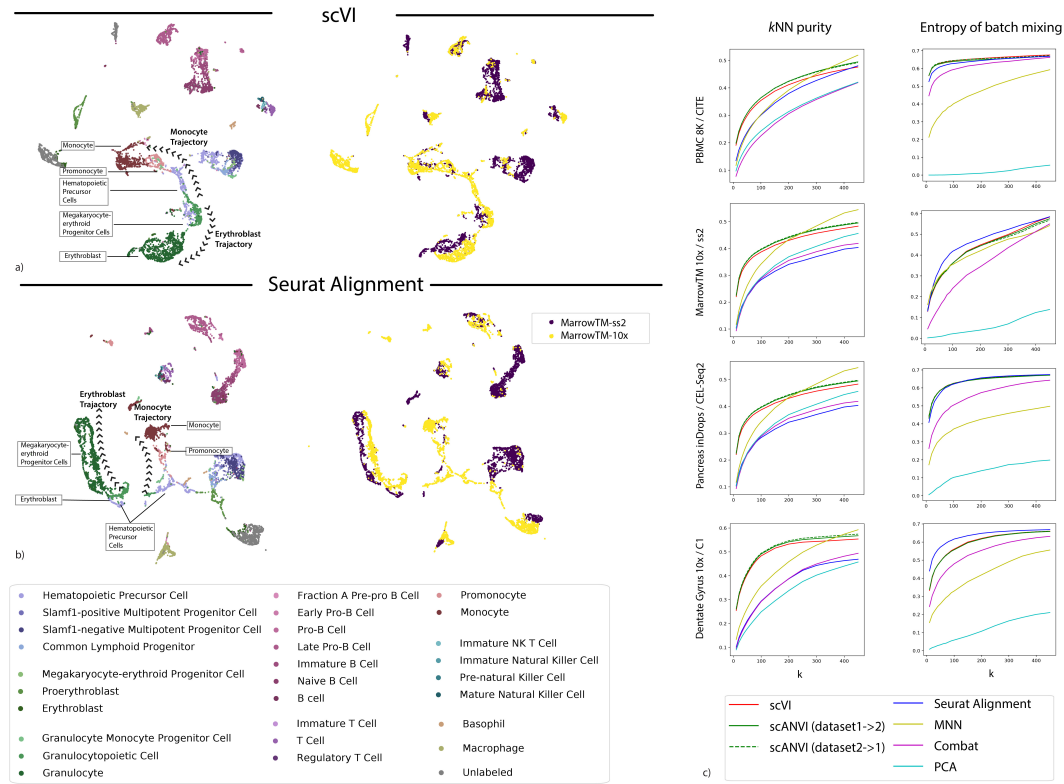
Figure 2: Benchmarking of scRNA-seq harmonization algorithms (*a*)Visualization of the latent space of scVI using Uniform Manifold Approximation and Projection (UMAP [42]) for the bone marrow dataset pair [9], colored by cell type and batches. (*b*) Visualization of the Seurat Alignment latent space of the same dataset. (*c*) Quantitative comparison of the performance of scVI and Seurat Alignment by two measures. One the left retainment of structure for the benchmark algorithms on the four pairs of dataset evaluated via the k-nearest neighbors purity, defined as a jaccard index of neighbor sets (**Online Methods**). On the right dataset mixing for the benchmark algorithms on the four pairs of datasets evaluated by entropy of batch mixing.

Harmonizing datasets with a different composition of cell types

One of the primary challenges of the harmonization problem is handling cases in which the cell types present in the input datasets only partially overlap or do no overlap at all. Since this is a plausible scenario in many applications, it is important to account for it and avoid over-normalizing or "forcing" distinct cell populations onto each other. To evaluate this, we performed several stress tests in which we artificially manipulated the composition of cell types in the input datasets prior to harmonization. As our benchmark method we use Seurat Alignment, which performed better than the remaining benchmark methods in our first round of evaluation (**Figure 2**).

As a case study, we used a pair of PBMC datasets (PBMC-CITE [25], PBMC-8K [33]) that initially contained a similar composition of immune cell types (**Supplementary Table 2**). We were first interested in the case of no biological overlap (**Figure 3a-d**). To test this, for a given cell type c_0 (e.g., natural killer cells), we only keep cells of this type in the PBMC-CITE dataset and remove all cells of this type from the PBMC-8K dataset. In **Figure 3a-b**, we show an example of UMAP visualization of the harmonized data, with natural killer cells as the left out cell type c_0. Evidently, when harmonizing the two perturbed datasets with scVI, the natural killer cells appear as a separate cluster and are not wrongly mixed with cells of different types from the other dataset. Conversely, we see a larger extent of mixing in the latent space inferred by Seurat Alignment. A more formal evaluation is provided in **Figure 3c-d**, which presents our two harmonization performance metrics for each cell type averaged across all perturbations (in each perturbation, c_0 is set to a different cell type). We also included scANVI with the true number of cell types ($C = 6$) in this analysis, using the cell labels from the PBMC-CITE dataset.

Under the ideal scenario of a successful harmonization, we expect both a low entropy of batch mixing (since the datasets do not overlap), and retainment of the original structure. Evidently, both scVI and scANVI exhibit a consistently low level of batch mixing that is better or comparable to that of Seurat Alignment, while retaining the original structure more accurately.

As an additional scenario, we investigated the case where the input datasets contain a similar set of cell types, with the exception of one cell type that appears in only one of the datasets. To simulate this, for a given cell type c_0, we removed cells of this type from the PBMC-8K dataset, and then harmonize the remaining cells with the unaltered PBMC-CITE (which still contains c_0). We show an example of UMAP visualization in **Figure 3e-f**, removing CD4+ T cells from the PBMC-8K dataset. Evidently, in the scVI latent space, the PBMC-CITE "unique" CD4+ T cell population is not wrongly mixed with cells from the perturbed PBMC-8K dataset, but rather appears as a distinct cluster. For a more formal analysis, **Figure 3g-i** shows the harmonization statistics for perturbing the six major cell types present in the PBMC datasets. As above, we also evaluated scANVI in this context, using the labels from the unperturbed (PBMC-CITE) dataset.

Figure 3g shows that the entropy of batch mixing from the "unique" populations (averaging over all six perturbations) is low in all three methods (scVI, scANVI and Seurat Alignment), with a slight advantage for scVI and scANVI. **Figure 3h-i** shows the harmonization statistics for each population, averaging over all shared cell types between the two datasets. Evidently, for the populations that are indeed common to the two datasets, scVI and scANVI are capable of mixing them properly, while preserving the original structure, comparing favorably to Seurat Alignment on both measures. Overall, the results of this analysis demonstrate that scVI and scANVI are capable of harmonizing datasets with very different compositions, while not forcing erroneous mixing. These results are consistent with the design of scVI and scANVI, which aim to maximize the likelihood of a joint generative model, without making *a priori* assumptions about the similarity in the composition of the input datasets.
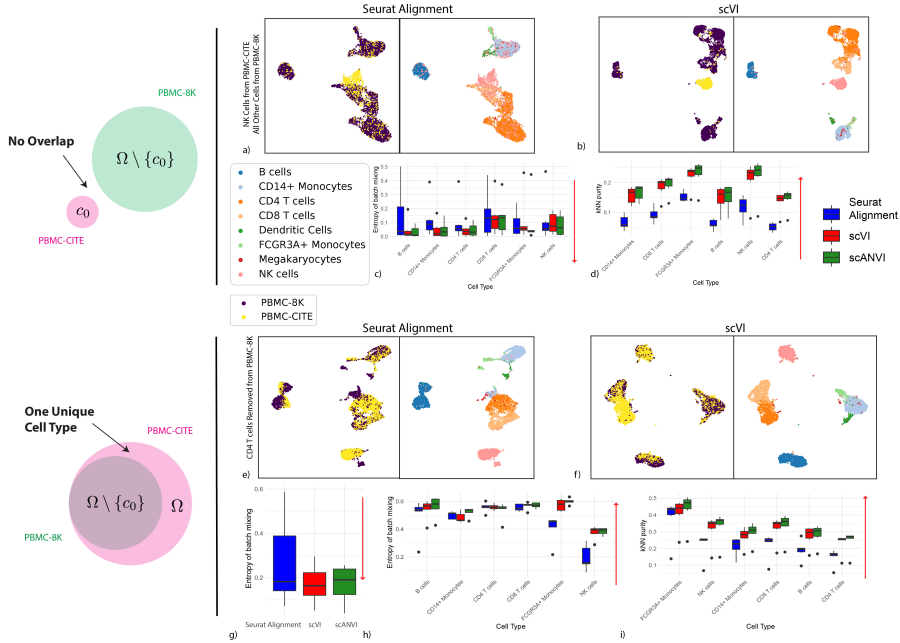
Figure 3: Harmonizing datasets with different cellular composition. $(a - d)$ show the case when no cell type is shared, where PBMC-8K contains all cells other than cell type c_0 and PBMC-CITE contains only cell type c_0. $(a - b)$ UMAP visualization for the case where c_0 corresponds to natural killer cells. $(c - d)$ Harmonization statistics, aggregating the six experiments (setting c_0 to a different cell type in each experiment). $(e - i)$ show the results of cell type c_0 is removed from the PBMC-8K dataset, while the PBMC-CITE dataset remains the same. $(e - f)$ UMAP visualization for the case where c_0 corresponds to CD4+ T cells. (g) batch entropy mixing for the cell type that was removed. (h) batch entropy mixing for each cell type in the 5 experiments where they were not removed. (i) Retainment of the original structure, aggregating all 6 experiments. Red arrows indicate the desired direction for each performance measure (e.g., low batch entropy is desirable in (d)). The boxplots are standard Tukey boxplots where the box is delineated by the first and third quartile and the whisker lines are the first and third quartile plus minus 1.5 times the box height. The dots are outliers that fall above or below the whisker lines.

Harmonizing continuous trajectories

While so far we considered datasets that have a clear stratification of cells into discrete sub-populations, a conceptually more challenging case is harmonizing datasets in which the major source of variation forms a continuum, which inherently calls for accuracy at a higher level of resolution.

To explore this, we use a pair of datasets that provide a snapshot of hematopoiesis in mice (HEMATO-Tusi [43], HEMATO-Paul [44]; **Figure 4**). These datasets consist of cells along the transition from common myeloid progenitor cells (**Figure 4a-b**; middle) through two primary differentiation trajectories myeloblast (top) and erythroblast-megakaryocyte (bottom). Notably, the HEMATO-Tusi dataset contains cells that appear to be more terminally differentiated, which are located at the extremes of the two primary branches. This can be discerned by the expression of marker genes (**Figure 4e**). For instance the HEMATO-Tusi unique erythroid cell population expresses *Hba-a2* (hemoglobin subunit) and *Alas2* (erythroid-specific mitochondrial 5-aminolevulinate synthase) that are known to be present in reticulocytes [45, 46]. At the other end, the granulocyte subset that is captured only by HEMATO-Tusi expresses *Itgam* and *S100a8*. *S100a8* is a neutrophil specific gene predicted by Nano-dissection [47] and is associated with GO processes such as leukocyte migration associated with inflammation and neutrophil aggregation. *Itgam* is not expressed in granulocyte-monocyte progenitor cells but is highly expressed in mature monocytes, mature eosinophils and macrophages [48]. We therefore do not expect mixing to take place along the entire trajectory. To account for this, we evaluated the extent of batch entropy mixing at different points along the harmonized developmental trajectory. As expected, we find that in most areas of the trajectory the two datasets are well mixed, while at the extremes, the entropy reduces significantly, using either scVI or Seurat Alignment (**Figure 4c**). Overall, we observe that scVI compares well in terms of both mixing the differentiation trajectories in each dataset and preserving their original, continuous, structure (**Figure 4a-d**).

To validate scANVI in this context as well, we provided it with the categorical labels of cells along the two developmental trajectories, indicating their cell state (**Figure 4c-d** and **Supplementary Figure 7**). Even though this labeling scheme does not explicitly account for the ordering between states, we observe that scANVI is capable of mixing the two datasets, while retaining their original structure, achieving a level of accuracy comparable to that of scVI and better than that of Seurat Alignment.
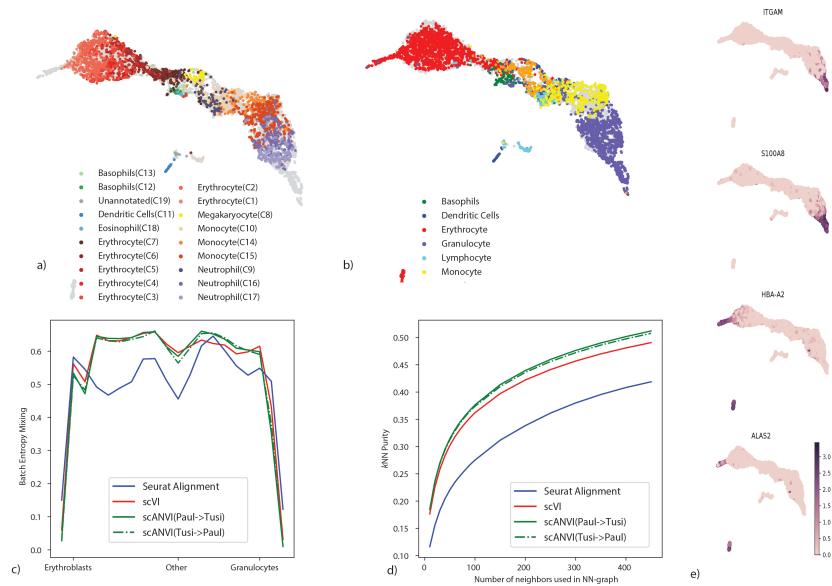
Figure 4: Harmonizing developmental trajectories. $(a - b)$ UMAP visualization of the scVI latent space, with cells colored by the original labels from either the HEMATO-Paul (a) or HEMATO-Tusi (b) studies. The cells from the other dataset are colored in gray. (c) Batch entropy mixing of 20 of bins HEMATO-Tusi cells ordered by the potential of each cell derived from the PBA algorithm used in the original publication. Potential is a pseudotime measure that describes how differentiated a cell is. (center: common myeloid progenitors; moving left: erythrocyte branch; moving right: granulocyte branch). (d) k-nearest neighbors purity for scVI, Seurat, and scANVI. (e) Expression of marker genes that help determine the identity of batch-unique cells.

Rapid integration of multiple datasets

To demonstrate the scalability of our framework in the context of harmonizing multiple (and possibly large) dataset, we ran scVI to integrate a cohort of 26 datasets spanning 105,476 cells from multiple tissues and technologies, which was made available by the authors of Scanorama (a scalable variant of MNN [19]). Using the hardware specified in the original paper [19] (Intel Xeon E5-2650v3 CPU limited to 10 cores with 384 GB of RAM), Seurat Alignment and MNN required over 24 hours, while Scanorama completed its run in 20 minutes. Using a simpler configuration (eight-core Intel i7-6820HQ CPU with 32 GB RAM) along with one NVIDIA Tesla K80 GPU (GK210GL; addressing 24 GB RAM), we found that scVI integrates all datasets and learns a common embedding in less than 50 minutes. Notably, this running time is competitive considering the reduced memory availability and the increased complexity of our model (compared to truncated singular value decomposition followed by the nearest neighbor matching algorithm in Scanorama). Notably, the latent space of scVI recapitulates well the major tissues and cell types (**Supplementary Figure 8**), and the position of cells in the latent space provides an effective predictor for the cell type label (**Supplementary Figure 8** and **Online Methods**).

Transferring cell type annotations between datasets

We next turned to evaluate scVI and scANVI in the context of harmonization-based annotation. Here, we test the extent to which annotations from a previously annotated dataset can be used to automatically derive annotations in a new unannotated dataset. For scVI and Seurat Alignment, we derive the annotations by first harmonizing the input datasets and then running a k-nearest neighbors classifier (setting k to 10) on the joint latent space, using the annotated cells to assign labels to the unannotated ones. Conversely, scANVI harmonizes the input datasets while using any amount of available labels. The prediction of unobserved labels is then conducted using the approximate posterior assignments $q_\Phi(c \mid z)$ of cell types (**Online Methods**), which can be derived directly from the model. An alternative approach, which we also include in our benchmark was taken by scmap-cluster [28], which instead of harmonizing, directly builds a classifier based on the labeled cells and then applies this classifier to the unlabeled cells.

We start by exploring the four dataset pairs in **Figure 2**, which have been annotated in their respective studies. In each experiment, we "hide" the cell type annotations from one dataset and transfer the second dataset labels to the first one. As a measure of performance, we report the weighted accuracy, which is the percent of cells that were correctly assigned to their correct (hidden) label, averaging over all labels (**Online Methods**). Importantly, the annotations in this first set of case studies were derived computationally. For example, by first clustering the cells, looking for marker genes expressed by each cluster and then assigning labels to the clusters accordingly. This level of annotation therefore makes the prediction problem relatively easy, and indeed, while we find that overall scANVI predicts unobserved labels more accurately, the differences between the methods are mild (**Supplementary Figures 9 and 10**).

To evaluate the accuracy of annotations without the need for computationally- derived labels, we turned to the PBMC-CITE dataset which includes measurements of ten key marker proteins in addition to mRNA [25], and the PBMC-sorted dataset [3], where cells were collected from bead purifications for eleven cell types (**Supplementary Table 3**). We applied scVI and scANVI to harmonize and annotate these two datasets along with a third dataset of PBMC (PBMC-68K [3]). Our analysis contains a combined set of $n = 169,850$ cells from the three datasets altogether. To generate a realistic scenario of cell type annotation, we only provide access to the experimentally-based labels from the PBMC-sorted dataset (**Figure 5a-c**). As an additional benchmark, we also evaluate Seurat Alignment, which was tested after removal of a randomly selected subset (40%) of the two large datasets (PBMC-68K and PBMC-sorted) due to scalability issues. Considering our harmonization performance measures (i.e., retainment of the original structure and batch mixing), we observe as before that scVI and scANVI perform similarly and compare favorably to Seurat Alignment. We then evaluated the accuracy of assigning unobserved labels, focusing on the PBMC-CITE dataset. Instead of using the labels from the original PBMC-CITE study as ground truth (which were computationally derived), we used the protein data, which provides an experimentally-derived proxy for cell state. To this end, we quantified the extent to which the similarity between cells in the harmonized mRNA-based latent space is consistent with their similarity at the protein level (**Online Methods**). We first computed the average discrepancy (sum of squared differences) between the protein measurements in each

cell and the average over its k-nearest neighbors. As a second measure we computed for each PBMC-CITE cell the overlap between its k-nearest PBMC-CITE neighbors in the harmonized mRNA-based space and in the protein space. We then report the average across all cells in **Supplementary Figure 11**. Evidently, scANVI outperformed both scVI and Seurat Alignment for a wide range of neighborhood sizes, providing a representation for the mRNA data that is more consistent with the protein data (**Figure 5c**).

As further support for the validity of these results, we confirmed that the labels inferred by scANVI in the PBMC-CITE dataset are consistent with the protein expression values (e.g., observing a uniquely high level of *CD19* expression in cells assigned with the "B cell" label; **Figure 5d** and **Supplementary Figure 11**). Interestingly, when considering the latent space learned by scANVI, we observed a certain amount of possible mislabeling in the original study of the PBMC-68K dataset (**Figure 5e**). In that study, the PBMC-68K cells were assigned with labels by taking the maximum correlation with cell subsets from the experimentally-annotated PBMC-sorted data. However this approach might be error prone, most likely due to low sensitivity and the influence of genes that are less relevant to cell type classification. Specifically, we observe a substantual amount of cells that are labeled by scANVI as T cells, but originally labeled as dendritic cells or natural killer cells. This re-annotation as T cells is supported by the expression of marker genes [49] of the respective cell subsets (**Supplementary Figure 11**).
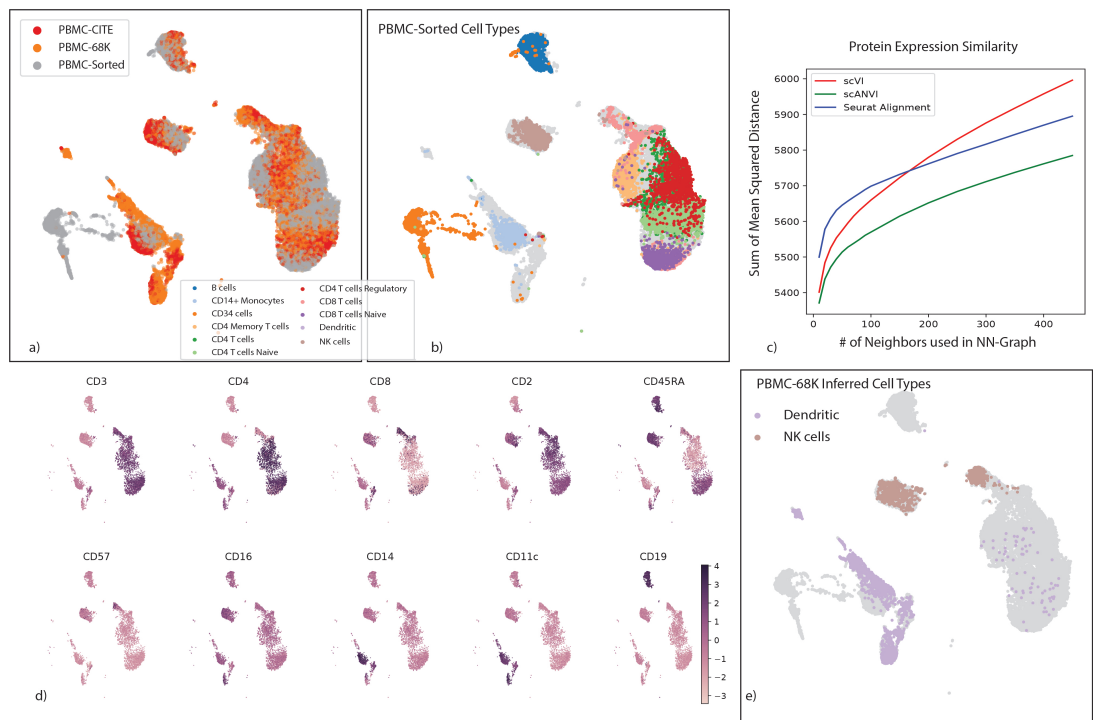
Figure 5: Validation of cell type annotations using additional metadata. (a-b) UMAP plot of the scANVI latent space inferred for three harmonized datasets: PBMC-CITE [25], PBMC-sorted [3], and PBMC-68K [3]. Cells are colored by the batch they come from (*a*) and the PBMC-sorted labels(*b*). Cells from the PBMC-Cite and PBMC-68K are colored gray in (*b*). (c) The consistency of the harmonized PBMC-CITE mRNA data with the respective protein measurements, evaluated by mean squared error and for different neighborhood size. Lower values indicate higher consistency. (*d*) UMAP plot of the scANVI latent space, where cells are colored by normalized protein measurement. Only PBMC-CITE cells are displayed. (*e*) UMAP plot of the scANVI latent space, with cells from the PBMC-68k dataset colored according to their original label. For clarity of presentation, only cells originally labeled as dendritic cells or natural killer cells are colored. Evidently, a large number of these cells are mapped to a cluster of T-cells (right side of the plot).

Cell type annotation in a single dataset based on "seed" labels

An important variant of the annotation problem lies within the context of an *ab initio* labeling of a single dataset where only a subset of the cells can be confidently annotated based on the raw data. This increasingly prevalent scenario may result from limited sensitivity of the scRNA-seq assay, where marker genes may only be confidently observed in a small subset of cells. One common way to address this problem is to compute some form of a distance metric between cells (e.g., after embedding with scVI or using Seurat PCA) and then assign labels based on proximity to annotated cells [3]. To benchmark our methods, we consider two such predictors: the first is clustering the cells and taking a majority vote inside each cluster, and the second is taking the majority vote of the k-nearest neighbors around each unannotated cell ($k = 10$). While these approaches are quite straightforward, their accuracy might suffer when the data does not form clear clusters [43], or when differences between labels are too subtle to be captured clearly by a transcriptome-wide similarity measure. To address these issues, scANVI takes an alternative approach, namely learning a latent embedding that is guided by the available labels, and then producing posterior probabilities for assigning labels to each cell.

As a case study, we compiled a dataset consisting of several experimentally sorted and labeled subsets of T cells from the PBMC-sorted dataset, including CD4 memory, CD4 naive, CD4 regulatory and CD8 naive. To make our analysis more realistic, we assume that the labels are completely unknown to us and therefore begin by trying to assign each T cell to its respective subset using marker genes (12 altogether; see **Online Methods**). Notably, several important biomarkers (*CD4*, *CTLA4*, and *GITR*) are detected in less than 5% of the cells, which renders their use for annotation not straightforward. Notably, many of these biomarkers are sparsely expressed to the extent that they are likely to be filtered out in the gene selection step of most harmonization procedures (**Figure 6a**).

To analyze this dataset, we first computed a signature score for each cell and for each label (i.e., T cell subset) using the scaled raw expression values of the respective marker genes (**Online Methods**). We then designated the top 50 scoring cells in each subset as the seed set of cells that are confidently annotated for that subset (**Figure 6b**). Reassuringly, this partial annotation is in agreement with the experimentally derived cell type labels available for this dataset (**Figure 6c**). However, this dataset does not form clear clusters, and in particular the seed sets of cells are not well separated. Such an observation makes clustering-based approaches potentially less precise. Indeed, using k-means clustering on the scVI and Seurat Alignment latent space, we find that 74% and 72% of the cells were assigned with their correct label. Similar analysis with two additional popular clustering algorithms (DBSCAN [50] and PhenoGraph [51]) further emphasizes the challenge of a cluster-based approach on this data. Specifically, DBSCAN does not partition the data into more than one cluster (scanning through a large number of parameter values; **Online Methods**), and PhenoGraph predicts 9 clusters and achieves an accuracy of 41% (**Supplementary Figure 12**).

Consistent with these results, the application of a k-nearest neighbors classifier resulted in a similar level of accuracy in the Seurat PCA latent space (71%), which is slightly improved when replacing it with the scVI latent space (73%; **Supplementary Figure 12**). Conversely, after fitting the scANVI model based on this partial labeling, the annotation posterior $q_\Phi(c \mid z)$ (**Figure 6d**) provides a substantially more accurate cell type assignment, with 84% of cells annotated correctly. The scANVI latent space also has more distinct cell type clusters than both scVI and Seurat Alignment (**Supplementary Figure 12**).
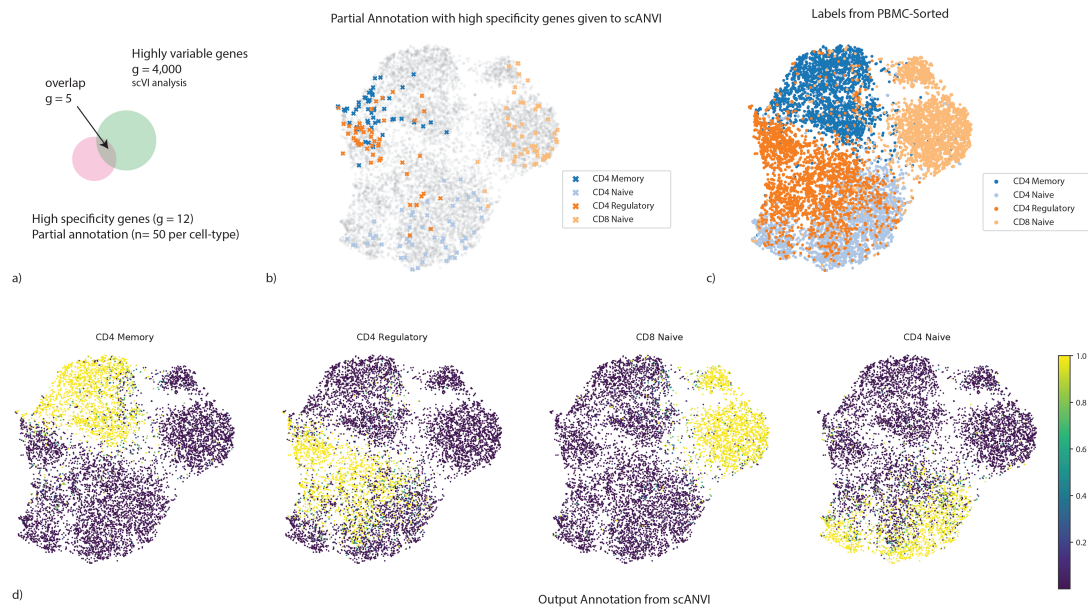
16

Figure 6: Cell type annotation in a single dataset using "seed" labeling. (*a*) discrepancies between marker genes that can be used to confidently label cells and highly variable genes in scRNA-seq analysis. (*b* − *d*) UMAP plot of the scVI latent space. (*b*) Seed cells are colored by their annotation (using known marker genes). (*c*) PBMC-sorted cell type labels from the original study based on marker-based sorting (*d*) The posterior probability of each cell being one of the four T cell subtypes obtained with scANVI.

Cell type taxonomy and hierarchical classification with scANVI

Another subtle yet important variation of the annotation problem is when the labels are not mutually exclusive but rather form a taxonomy of cell types or states. To effectively annotate cells in this setting, we extended scANVI to perform hierarchical classification, which as before we carry out from first principles, relying on probabilistic graphical models (**Supplementary Note 4**). To demonstrate this extended version, we use a dataset of the mouse nervous system [52] that was annotated using a cell type taxonomy with several levels of granularity. At the lowest (most granular) level, the cells are stratified into 265 sub-types. At the second lowest level of granularity these 265 sub-types are grouped into 39 subsets, each corresponding to a coarser cell type definition.

We evaluate the ability of scANVI as well as competing methods at inferring these granular labels when provided with partial "seed" annotation — namely label information for 5 randomly selected cells per label (which accounts for an overall of 0.8% of the cells). We first observe that Seurat PCA followed by a k-nearest neighbors classifier provides a weighted accuracy of 23% (averaging over all cell types). scVI provides a substantially better, yet still lower level of accuracy at 32%. Interestingly, when scANVI is used without accounting for hierarchy, its performance is similar to the unsupervised scVI (at 32%), which might result from very large number of labels that may require hyperparameter tuning (e.g., increasing the number of classifier training epochs; see **Supplementary Note 3**). However, when we take the hierarchy of the labels into account, the performance of scANVI increases to 37%, thus outperforming the other methods. Notably, while we tested the extrapolation of seed labeling and the hierarchical mode only in the context of a single dataset, this variation of the scANVI model can also be directly applied in the context of multiple datasets (i.e., transferring hierarchical annotations between datasets).

Hypotheses testing in harmonized datasets: the case of differential expression

With their probabilistic representation of the data, scVI and scANVI each provide a natural way of performing various types of hypotheses testing (**Online Methods**). This is different from other approaches [12, 13, 18, 19, 20] where the dataset alignment procedures do not carry direct probabilistic interpretation, and the resulting harmonized data can thus not be directly used for these purposes.

To demonstrate this, we focus on the problem of differential expression. As a case study, we use two PBMC datasets (PBMC-8K and PBMC-68K) where we assume that only one of the datasets (PBMC-8K) comes with prior annotation of cell types. We looked for differentially expressed genes in two settings: comparing the subpopulation of B cells to that of dendritic cells, and similarly for the CD4+ versus the CD8+ T cell subsets. For evaluation, we used reference sets of differentially expressed genes that were obtained from published bulk-level analysis of similar cell subsets [53, 54], as in [29].

To conduct a post-harmonization differential expression analysis with scVI, we first harmonized the two PBMC datasets and transferred labels from the PBMC-8K to the PBMC-68K using a k-nearest neighbors classifier on the joint latent space ($k = 10$). We then consider these annotations (predicted and pre-labeled) as fixed and sample 100 cell pairs, each pair consisting of one cell from each population. For each cell pair we sample gene expression values from the variational posterior, while marginalizing over the different datasets, to compute the probability for differential expression in a dataset-agnostic manner. Aggregating across all selected pairs results in Bayes factors that reflect the evaluated extent of differential expression (**Online Methods**). Since scANVI assigns posterior probability for associating any cell to any label, it enables a more refined scheme. Specifically, instead of sampling pairs of cells we are sampling pairs of points in the latent space, while conditioning on the respective label. This approach therefore does not assume a fixed label for each cell (or point in latent space) as in the scVI scheme, but rather a distribution of possible labelsthus making it potentially more robust to mis-annotation. As an additional benchmark method, we included edgeR [55], which was shown to perform well on scRNA-seq data [56] and uses a log-linear model to control for technical sample-to-sample variation.

For evaluation, we first defined genes as true positives if their adjusted p-values in the reference bulk data were under 5% and then calculated the area under the ROC curve (AUROC) based

on the Bayes factors (for scVI and scANVI) or the p-values (for edgeR). Since defining true positives requires a somewhat arbitrary threshold, we also used a second score that evaluates the reproducibility of gene ranking (bulk reference vs. single-cell; considering all genes), using the Kendall rank correlation coefficient (**Supplementary Figure 13**). As a reference, we look at the accuracy of differential expression analysis in each PBMC dataset separately (using their prior annotations to define the sets of cells we are comparing), computed with scVI (as in [29]) and edgeR. Reassuringly, we find that the performance of scVI on the joint data is not lower than it is in either dataset in isolation. We also find that in both case studies, scVI performs moderately better than scANVI, which is to be expected as scANVI has a more complex model, yet in our case studies this added complexity is not critical since the unobserved labels are relatively easy to predict (**Supplementary Figure 9**). Importantly however, we observe that both scANVI and scVI compare favorably to edgeR in their accuracy and are thus capable of conducting differential expression effectively in the context of multiple datasets.

Discussion

In this study, we demonstrated that scVI provides a principled approach to scRNA-seq data harmonization through joint probabilistic representation of multiple dataset, while accounting for technical hurdles such as over-dispersion, variable library size and limited sensitivity. We have demonstrated that scVI compares favorably to other methods in its accuracy and that it scales well, not only in terms of the number of cells (as in [29]) but also the number of input datasets (as opposed to other methods that work in a pairwise fashion and therefore scale quadratically with dataset size [19]). We have also shown that the harmonization step of scVI provides an effective baseline for automated transfer of cell type labels, from annotated datasets to new ones.

While the performance of scVI in the annotation problem compares favorably to other algorithms, it does not make use of any existing cell state annotations during model training, but rather after the latent space has been learned. To make better use of these annotations (which may be available for only some of the input datasets or only some cells within a dataset), we developed scANVI, a semi-supervised variant of scVI. While the latent space of scVI is defined by a Gaussian vector with diagonal unit variance, scANVI uses a mixture model, which enables it to directly represent the different cell states (each corresponding to a mixture component; see **Online Methods**) and provide a posterior probability of associating each cell with each label. We have demonstrated that similar to scVI, scANVI is capable of harmonizing datasets effectively. In addition, scANVI provides a way to address a number of variants of the annotation problem. Here, we have shown that it performs well in the most prevalent application of transferring labels from a reference dataset to an unannotated one, and that spurious annotations (when datasets do not overlap) are associated with low probability. We then demonstrated that scANVI can be used in the context of a single unannotated dataset, where high confidence ("seed") labels are first inferred for a few cells (using marker genes) and then propagated to the remaining cells. Finally, we showed that scANVI is especially useful in the challenging case where the differences between cell states are too subtle to be captured clearly by a transcriptome-wide similarity measure, as well as in the case where the labels are organized in a hierarchy.

One concern in applying methods based on neural networks [21, 57, 58, 59, 60] in single-cell genomics and other domains is the robustness to hyperparameters choices [61]. This concern has been addressed to some extent by recent progress in the field, proposing search algorithms based on held-out log-likelihood maximization [59]. In this manuscript, we used an alternative approach that is more conducive for direct and easy application of our methods - namely we fix the hyperparameters and achieve state-of-the-art results on a substantial number of datasets and case studies.

Another important consideration while designing statistical models is the trade-off between goodness of fit and interpretability, which is still an open topic in machine learning research. Simple models such as the latent Dirichlet allocation [62] might not be particularly suited for scRNA-seq noise but are yet of interest, e.g., due to the immediate interpretation of word-level (i.e., gene-level) contributions to topics (i.e., cell types) [63]. Further effort in the use of deep generative models for applications in computational biology should come with attempts to perform model interpretation. For instance, SAUCIE [21] experimentally proposes to add an entropy regularization to a hidden layer of its denoising auto-encoder in order to infer clustering. Future principled efforts may focus on putting a suitable prior such as sparsity on neural networks

weights (e.g., as in [64]). That way, individual neurons of the last hidden layer of the generative model would correspond to individual gene modules, directly readable from the weight sparsity motifs. Finally, as recent preprints propose proof of concepts for integrating single cell data across different data modalities such as Single molecule fluorescent in situ hybridization (smFISH), RNA-seq, ATAC-seq and DNA methylation [18, 20], further work can utilize probabilistic graphical models that quantify measurement uncertainties in each assay, as well as the uncertainties of transferring information between modalities (e.g., predicting unmeasured gene expression in smFISH data).

An important distinguishing feature of both scVI and scANVI is that they rely on a fully-probabilistic model, thus providing a way to directly propagate uncertainties to any downstream analysis. While we have demonstrated this for differential expression analysis and cell type annotation, this can be incorporated to other tasks, such as differential abundance of sub-populations in case-control studies, correlation between genes and more. We therefore expect scVI, scANVI and similar tools to be of much interest as the field moves toward the goal of increasing reproducibility and consistency between studies and converging on to a common ontology of cell types. Both scVI and scANVI are available as an open-source software at https://github.com/YosefLab/scVI. The code for reproducing the results in this manuscript has been deposited at https://doi.org/10.5281/zenodo.2529945.

Acknowledgments

Author contributions

RL, EM, JR and NY conceived the statistical model. EM developed the software. CX, RL and EM applied the software to real data analysis. CX, RL, JR, NY, and MIJ wrote the manuscript. NY and MIJ supervised the work.

Competing interests

The authors declare no competing interests.

References

[1] A. Tanay and A. Regev, "Scaling single-cell genomics from phenomenology to mechanism," *Nature*, vol. 541, no. 7637, pp. 331–338, 2017.

[2] E. Macosko, A. Basu, R. Satija, J. Nemesh, K. Shekhar *et al.*, "Highly parallel genome-wide expression profiling of individual cells using nanoliter droplets," *Cell*, vol. 161, no. 5, pp. 1202–1214, 2017.

[3] G. X. Zheng, J. M. Terry, P. Belgrader, P. Ryvkin, Z. W. Bent, R. Wilson, S. B. Ziraldo, T. D. Wheeler, G. P. McDermott, J. Zhu *et al.*, "Massively parallel digital transcriptional profiling of single cells," *Nature communications*, vol. 8, p. 14049, 2017.

[4] S. Semrau, J. E. Goldmann, M. Soumillon, T. S. Mikkelsen, R. Jaenisch, and A. Van Oudenaarden, "Dynamics of lineage commitment revealed by single-cell transcriptomics of differentiating embryonic stem cells," *Nature Communications*, vol. 8, no. 1, p. 1096, 2017.

[5] J. T. Gaublomme, N. Yosef, Y. Lee, R. S. Gertner *et al.*, "Single-cell genomics unveils critical regulators of Th17 cell pathogenicity," *Cell*, vol. 163, no. 6, pp. 1400–1412, 2015.

[6] A. P. Patel, I. Tirosh, J. J. Trombetta, A. K. Shalek, S. M. Gillespie, H. Wakimoto, D. P. Cahill, B. V. Nahed, W. T. Curry, R. L. Martuza, D. N. Louis, O. Rozenblatt-Rosen, M. L. Suvà, A. Regev, and B. E. Bernstein, "Single-cell RNA-seq highlights intratumoral heterogeneity in primary glioblastoma," *Science*, vol. 344, no. 6190, pp. 1396–1401, jun 2014.

[7] P. Angerer, L. Simon, S. Tritschler, F. A. Wolf, D. Fischer, and F. J. Theis, "Single cells make big data: New challenges and opportunities in transcriptomics," *Current Opinion in Systems Biology*, vol. 4, pp. 85 – 91, 2017.

[8] A. Regev, S. A. Teichmann, E. S. Lander, I. Amit, C. Benoist *et al.*, "The human cell atlas," *eLife*, vol. 6, p. e27041, dec 2017.

[9] S. R. Quake, T. Wyss-Coray, S. Darmanis, T. M. Consortium *et al.*, "Single-cell transcriptomic characterization of 20 organs and tissues from individual mice creates a tabula muris," *bioRxiv*, p. 237446, 2018.

[10] "Brain initiative cell census network (biccn)," 2018. [Online]. Available: https://biccn.org/data/

[11] L. Wen and F. Tang, "Boosting the power of single-cell analysis," *Nature Biotechnology*, vol. 36, p. 408, May 2018.

[12] L. Haghverdi, A. T. L. Lun, M. D. Morgan, and J. C. Marioni, "Batch effects in single-cell RNA-sequencing data are corrected by matching mutual nearest neighbors," *Nature Biotechnology*, vol. 36, no. 5, pp. 421–427, 2018.

[13] A. Butler, P. Hoffman, P. Smibert, E. Papalexi, and R. Satija, "Integrating single-cell transcriptomic data across different conditions, technologies, and species," *Nature Biotechnology*, vol. 36, p. 411, Apr 2018.

[14] A. Wagner, A. Regev, and N. Yosef, "Revealing the vectors of cellular identity with single-cell genomics," *Nature Biotechnology*, vol. 34, no. 11, pp. 1145–1160, 2016.

[15] W. E. Johnson, C. Li, and A. Rabinovic, "Adjusting batch effects in microarray expression data using empirical Bayes methods," *Biostatistics*, vol. 8, no. 1, pp. 118–127, 2007.

[16] M. E. Ritchie, B. Phipson, D. Wu, Y. Hu, C. W. Law, W. Shi, and G. K. Smyth, "limma powers differential expression analyses for rna-sequencing and microarray studies," *Nucleic Acids Res*, vol. 43, no. 7, pp. e47–e47, Apr 2015.

[17] D. Risso, F. Perraudeau, S. Gribkova, S. Dudoit, and J.-P. Vert, "A general and flexible method for signal extraction from single-cell RNA-seq data," *Nature Communications*, vol. 9, p. 284, 2018.

[18] J. Welch, V. Kozareva, A. Ferreira, C. Vanderburg, C. Martin, and E. Macosko, "Integrative inference of brain cell similarities and differences from single-cell genomics," *bioRxiv*, 2018. [Online]. Available: https://www.biorxiv.org/content/early/2018/11/02/459891

[19] B. L. Hie, B. Bryson, and B. Berger, "Panoramic stitching of heterogeneous single-cell transcriptomic data," *bioRxiv*, 2018. [Online]. Available: https://www.biorxiv.org/content/early/2018/07/17/371179

[20] T. Stuart, A. Butler, P. Hoffman, C. Hafemeister, E. Papalexi, W. M. Mauck, M. Stoeckius, P. Smibert, and R. Satija, "Comprehensive integration of single cell data," *bioRxiv*, 2018. [Online]. Available: https://www.biorxiv.org/content/early/2018/11/02/460147

[21] M. Amodio, K. Srinivasan, D. van Dijk, H. Mohsen, K. Yim, R. Muhle, K. R. Moon, S. Kaech, R. Sowell, R. Montgomery, J. Noonan, G. Wolf, and S. Krishnaswamy, "Exploring Single-Cell Data with Multitasking Deep Neural Networks," *bioRxiv*, 2017. [Online]. Available: https://www.biorxiv.org/content/early/2017/12/19/237065

[22] U. Shaham, K. P. Stanton, J. Zhao, H. Li, K. Raddassi, R. Montgomery, and Y. Kluger, "Removal of batch effects using distribution-matching residual networks," *Bioinformatics*, vol. 33, no. 16, pp. 2539–2546, 2017.

[23] D. DeTomaso, M. Jones, M. Subramaniam, T. Ashuach, C. J. Ye, and N. Yosef, "Functional interpretation of single-cell similarity maps," *bioRxiv*, 2018. [Online]. Available: https://www.biorxiv.org/content/early/2018/08/29/403055

[24] D. DeTomaso and N. Yosef, "FastProject: A tool for low-dimensional analysis of single-cell RNA-seq data," *BMC Bioinformatics*, no. 1, p. 315, dec 2016.

[25] M. Stoeckius, C. Hafemeister, W. Stephenson, B. Houck-Loomis, P. K. Chattopadhyay, H. Swerdlow, R. Satija, and P. Smibert, "Simultaneous epitope and transcriptome measurement in single cells," *Nature methods*, vol. 14, no. 9, p. 865, 2017.

[26] C. Weinreb, A. E. Rodriguez-Fraticelli, F. D. Camargo, and A. M. Klein, "Lineage tracing on transcriptional landscapes links state to fate during differentiation," *bioRxiv*, 2018. [Online]. Available: https://www.biorxiv.org/content/early/2018/11/11/467886

[27] F. Wagner and I. Yanai, "Moana: A robust and scalable cell type classification framework for single-cell RNA-Seq data," *bioRxiv*, 2018. [Online]. Available: https://www.biorxiv.org/content/early/2018/10/30/456129

[28] V. Y. Kiselev, A. Yiu, and M. Hemberg, "scmap: projection of single-cell RNA-seq data across data sets," *Nature Methods*, vol. 15, p. 359, Apr 2018.

[29] R. Lopez, J. Regier, M. B. Cole, M. Jordan, and N. Yosef, "Deep Generative Modeling for Single-cell Transcriptomics," *Nature Methods*, 2018.

[30] D. P. Kingma and M. Welling, "Auto-encoding variational Bayes," in *The International Conference on Learning Representations*, 2014.

[31] C. Louizos, K. Swersky, Y. Li, M. Welling, and R. Zemel, "The Variational Fair Autoencoder," in *International Conference on Learning Representations*, 2016.

[32] V. Nygaard, E. A. Rødland, and E. Hovig, "Methods that remove batch effects while retaining group differences may lead to exaggerated confidence in downstream analyses," *Biostatistics*, vol. 17, no. 1, pp. 29–39, Jan 2016.

[33] "10x genomics," 2017. [Online]. Available: https://support.10xgenomics.com/single-cell-gene-expression/datasets

[34] S. Picelli, O. R. Faridani, Å. K. Björklund, G. Winberg, S. Sagasser, and R. Sandberg, "Full-length rna-seq from single cells using smart-seq2," *Nature protocols*, vol. 9, no. 1, p. 171, 2014.

[35] Y. Xin, J. Kim, M. Ni, Y. Wei, H. Okamoto, J. Lee, C. Adler, K. Cavino, A. J. Murphy, G. D. Yancopoulos *et al.*, "Use of the fluidigm c1 platform for rna sequencing of single mouse pancreatic islet cells," *Proceedings of the National Academy of Sciences*, vol. 113, no. 12, pp. 3293–3298, 2016.

[36] D. A. Jaitin, E. Kenigsberg, H. Keren-Shaul, N. Elefant, F. Paul, I. Zaretsky, A. Mildner, N. Cohen, S. Jung, A. Tanay *et al.*, "Massively parallel single-cell rna-seq for marker-free decomposition of tissues into cell types," *Science*, vol. 343, no. 6172, pp. 776–779, 2014.

[37] A. M. Klein, L. Mazutis, I. Akartuna, N. Tallapragada, A. Veres, V. Li, L. Peshkin, D. A. Weitz, and M. W. Kirschner, "Droplet barcoding for single-cell transcriptomics applied to embryonic stem cells," *Cell*, vol. 161, no. 5, pp. 1187–1201, 2015.

[38] T. Hashimshony, N. Senderovich, G. Avital, A. Klochendler, Y. de Leeuw, L. Anavy, D. Gennert, S. Li, K. J. Livak, O. Rozenblatt-Rosen *et al.*, "Cel-seq2: sensitive highly-multiplexed single-cell rna-seq," *Genome biology*, vol. 17, no. 1, p. 77, 2016.

[39] C. Ziegenhain, B. Vieth, S. Parekh, B. Reinius, A. Guillaumet-Adkins, M. Smets, H. Leonhardt, H. Heyn, I. Hellmann, and W. Enard, "Comparative analysis of single-cell rna sequencing methods," *Molecular Cell*, vol. 65, no. 4, pp. 631–643.e4, Feb 2017.

[40] M. Baron, A. Veres, S. L. Wolock, A. L. Faust, R. Gaujoux, A. Vetere, J. H. Ryu, B. K. Wagner, S. S. Shen-Orr, A. M. Klein *et al.*, "A single-cell transcriptomic map of the human and mouse pancreas reveals inter-and intra-cell population structure," *Cell systems*, vol. 3, no. 4, pp. 346–360, 2016.

[41] H. Hochgerner, A. Zeisel, P. Lönnerberg, and S. Linnarsson, "Conserved properties of dentate gyrus neurogenesis across postnatal development revealed by single-cell rna sequencing," *Nature neuroscience*, vol. 21, no. 2, p. 290, 2018.

[42] L. McInnes and J. Healy, "UMAP: Uniform Manifold Approximation and Projection for Dimension Reduction," *arXiv*, Feb. 2018.

[43] B. K. Tusi, S. L. Wolock, C. Weinreb, Y. Hwang, D. Hidalgo, R. Zilionis, A. Waisman, J. R. Huh, A. M. Klein, and M. Socolovsky, "Population snapshots predict early haematopoietic and erythroid hierarchies," *Nature*, vol. 555, no. 7694, pp. 54–60, 2 2018.

[44] F. Paul, Y. Arkin, A. Giladi, D. Jaitin, E. Kenigsberg, H. Keren-Shaul, D. Winter, D. Lara-Astiaso, M. Gury, A. Weiner, E. David, N. Cohen, F. Lauridsen, S. Haas, A. Schlitzer, A. Mildner, F. Ginhoux, S. Jung, A. Trumpp, B. Porse, A. Tanay, and I. Amit, "Transcriptional heterogeneity and lineage commitment in myeloid progenitors," *Cell*, vol. 163, no. 7, pp. 1663 – 1677, 2015.

[45] S.-H. Goh, M. Josleyn, Y. T. Lee, R. L. Danner, R. B. Gherman, M. C. Cam, and J. L. Miller, "The human reticulocyte transcriptome," *Physiological genomics*, vol. 30, no. 2, pp. 172–178, 2007.

[46] "Transcription profiling by high throughput sequencing of murine hematopoietic progenitors and lineage cells." [Online]. Available: https://www.ebi.ac.uk/gxa/experiments/E-MTAB-3079/Results

[47] W. Ju, C. S. Greene, F. Eichinger, V. Nair, J. B. Hodgin, M. Bitzer, Y.-s. Lee, Q. Zhu, M. Kehata, M. Li *et al.*, "Defining cell-type specificity at the transcriptional level in human disease," *Genome research*, pp. gr–155 697, 2013.

[48] I. Papatheodorou, N. A. Fonseca, M. Keays, Y. A. Tang, E. Barrera, W. Bazant, M. Burke, A. Füllgrabe, A. M.-P. Fuentes, N. George *et al.*, "Expression atlas: gene and protein expression across multiple studies and organisms," *Nucleic acids research*, vol. 46, no. D1, pp. D246–D251, 2017.

[49] T. S. P. Heng, M. W. Painter, T. I. G. P. Consortium, K. Elpek, V. Lukacs-Kornek, N. Mauermann, S. J. Turley, D. Koller, F. S. Kim, A. J. Wagers, N. Asinovski, S. Davis, M. Fassett, M. Feuerer, D. H. D. Gray, S. Haxhinasto, J. A. Hill, G. Hyatt, C. Laplace, K. Leatherbee, D. Mathis, C. Benoist, R. Jianu, D. H. Laidlaw, J. A. Best, J. Knell, A. W. Goldrath, J. Jarjoura, J. C. Sun, Y. Zhu, L. L. Lanier, A. Ergun, Z. Li, J. J. Collins, S. A. Shinton, R. R. Hardy, R. Friedline, K. Sylvia, and J. Kang, "The immunological genome project: networks of gene expression in immune cells," *Nature Immunology*, vol. 9, p. 1091, Oct 2008.

[50] M. Ester, H.-P. Kriegel, J. Sander, and X. Xu, "A density-based algorithm for discovering clusters a density-based algorithm for discovering clusters in large spatial databases with noise," in *Proceedings of the Second International Conference on Knowledge Discovery and Data Mining*, 1996, pp. 226–231.

[51] J. H. Levine, E. F. Simonds, S. C. Bendall, K. L. Davis, E. ad D. Amir, M. D. Tadmor, O. Litvin, H. G. Fienberg, A. Jager, E. R. Zunder, R. Finck, A. L. Gedman, I. Radtke, J. R. Downing, D. Pe'er, and G. P. Nolan, "Data-driven phenotypic dissection of AML reveals progenitor-like cells that correlate with prognosis," *Cell*, vol. 162, no. 1, pp. 184–197, jul 2015.

[52] A. Zeisel, H. Hochgerner, P. Lönnerberg, A. Johnsson, F. Memic, J. van der Zwan, M. Häring, E. Braun, L. E. Borm, G. La Manno, S. Codeluppi, A. Furlan, K. Lee, N. Skene, K. D. Harris, J. Hjerling-Leffler, E. Arenas, P. Ernfors, U. Marklund, and S. Linnarsson, "Molecular architecture of the mouse nervous system," *Cell*, Aug 2018.

[53] H. I. Nakaya, J. Wrammert, E. K. Lee, L. Racioppi *et al.*, "Systems biology of vaccination for seasonal influenza in humans," *Nature Immunology*, vol. 12, no. 8, pp. 786–795, 7 2011.

[54] G. Görgün, T. A. W. Holderried, D. Zahrieh, D. Neuberg, and J. G. Gribben, "Chronic lymphocytic leukemia cells induce changes in gene expression of CD4 and CD8 T cells," *The Journal of Clinical Investigation*, vol. 115, no. 7, pp. 1797–805, 2005.

[55] M. D. Robinson, D. J. McCarthy, and G. K. Smyth, "edger: a bioconductor package for differential expression analysis of digital gene expression data," *Bioinformatics*, vol. 26, no. 1, pp. 139–140, 2010.

[56] C. Soneson and M. D. Robinson, "Bias, robustness and scalability in single-cell differential expression analysis," *Nature methods*, vol. 15, no. 4, p. 255, 2018.

[57] J. Ding, A. Condon, and S. P. Shah, "Interpretable dimensionality reduction of single cell transcriptome data with deep generative models," *Nature Communications*, vol. 9, no. 1, p. 2002, dec 2018.

[58] D. Wang and J. Gu, "VASC: Dimension reduction and visualization of single cell RNA sequencing data by deep variational autoencoder," *bioRxiv*, 2017. [Online]. Available: https://www.biorxiv.org/content/early/2017/10/06/199315

[59] G. Eraslan, L. M. Simon, M. Mircea, N. S. Mueller, and F. J. Theis, "Single cell RNA-seq denoising using a deep count autoencoder," *bioRxiv*, 2018. [Online]. Available: https://www.biorxiv.org/content/early/2018/04/13/300681

[60] C. H. Grønbech, M. F. Vording, P. N. Timshel, C. K. Sønderby, T. H. Pers, and O. Winther, "scVAE: Variational auto-encoders for single-cell gene expression data," *bioRxiv*, 2018. [Online]. Available: https://www.biorxiv.org/content/early/2018/05/16/318295

[61] Q. Hu and C. S. Greene, "Parameter tuning is a key part of dimensionality reduction via deep variational autoencoders for single cell rna transcriptomics," *bioRxiv*, 2018. [Online]. Available: https://www.biorxiv.org/content/early/2018/09/20/385534

[62] D. M. Blei, A. Y. Ng, and M. I. Jordan, "Latent dirichlet allocation," *Journal of Machine Learning Research*, vol. 3, pp. 993–1022, Mar. 2003.

[63] D. A. duVerle, S. Yotsukura, S. Nomura, H. Aburatani, and K. Tsuda, "CellTree: an R/bioconductor package to infer the hierarchical structure of cell populations from single-cell RNA-seq data," *BMC Bioinformatics*, Sep 2016.

[64] A. J. Riesselman, J. B. Ingraham, and D. S. Marks, "Deep generative models of genetic variation capture the effects of mutations," *Nature Methods*, vol. 15, no. 10, pp. 816–822, 2018. [Online]. Available: https://doi.org/10.1038/s41592-018-0138-4

[65] D. P. Kingma, S. Mohamed, D. Jimenez Rezende, and M. Welling, "Semi-supervised Learning with Deep Generative Models," in *Advances in Neural Information Processing Systems 27*, 2014, pp. 3581–3589.

[66] D. P. Kingma and J. Ba, "Adam: A method for stochastic optimization," in *International Conference on Learning Representations*, 2015.

[67] C. K. Sønderby, T. Raiko, L. Maaløe, S. K. Sønderby, and O. Winther, "Ladder variational autoencoders," in *Advances in Neural Information Processing Systems*, 2016.

[68] S. Ioffe and C. Szegedy, "Batch normalization: accelerating deep network training by reducing internal covariate shift," in *International Conference on Machine Learning*, 2015.

[69] L. Held and M. Ott, "On p-values and Bayes factors," *Annual Review of Statistics and Its Application*, vol. 5, no. 1, pp. 393–419, 2018.

[70] R. E. Kass, A. E. Raftery, S. Association, and N. Jun, "Bayes factors," *Journal of the American Statistical Association*, vol. 90, no. 430, pp. 773–795, 1995.

[71] T. S. Andrews and M. Hemberg, "Dropout-based feature selection for scRNASeq," *bioRxiv*, 2018. [Online]. Available: https://www.biorxiv.org/content/early/2018/05/17/065094

[72] M. B. Cole, D. Risso, A. Wagner, D. DeTomaso, J. Ngai, E. Purdom, S. Dudoit, and N. Yosef, "Performance assessment and selection of normalization procedures for single-cell RNA-seq," *bioRxiv*, 2017. [Online]. Available: https://www.biorxiv.org/content/early/2018/05/18/235382

[73] M. J. Muraro, G. Dharmadhikari, D. Grün, N. Groen, T. Dielen, E. Jansen, L. van Gurp, M. A. Engelse, F. Carlotti, E. J. de Koning *et al.*, "A single-cell transcriptome atlas of the human pancreas," *Cell systems*, vol. 3, no. 4, pp. 385–394, 2016.

[74] C. A. Vallejos, D. Risso, A. Scialdone, S. Dudoit, and J. C. Marioni, "Normalizing single-cell RNA sequencing data: challenges and opportunities," *Nature Methods*, pp. 565–571, 2017.

[75] R. Lopez, J. Regier, M. I. Jordan, and N. Yosef, "Information Constraints on Auto-Encoding Variational Bayes," *Advances in Neural Information Processing Systems*, 2018.

[76] A. Gretton, K. M. Borgwardt, M. J. Rasch, B. Schölkopf, and A. Smola, "A Kernel Two-Sample Test," *Journal of Machine Learning Research*, vol. 13, pp. 723–773, 2012.

[77] M. Langevin, E. Mehlman, J. Regier, R. Lopez, M. I. Jordan, and N. Yosef, "A deep generative model for semi-supervised classification with noisy labels," *arXiv*, vol. abs/1809.05957, 2018. [Online]. Available: http://arxiv.org/abs/1809.05957

23

Online Methods

scANVI: an extension to scVI for harmonization through semi-supervised annotation

scVI is a hierarchical Bayesian model [29] for single-cell RNA sequencing data with conditional distributions parametrized by neural networks. The graphical model of scVI (**Figure 1c**) is designed to disentangle technical signal (i.e., library size discrepancies, batch effects) and biological signal. We propose in this manuscript an extension of the scVI model to include information about cell types in the generative model. We name this extension scANVI (single cell ANnotation using Variational Inference). In our generative model, we assume each cell n is an independent realization of the following generative process.

Let K be the number of datasets and C be the number of cell types across all datasets (including cell types that are not observed). Let $\mathbf{c}$ describe the expected proportion of cells for each cell type. We use a non-informative prior $\mathbf{c} = \frac{1}{C}$ for this parameter. Latent variable

$$c_n \sim \text{Multinomial}(\mathbf{c})$$

describes the cell type of the cell n. Latent variable

$$u_n \sim \mathcal{N}(0, I)$$

is a low-dimensional random vector describing cell n within its cell type. Conceptually, this random variable could describe cell-cycles or sub-cell types. By combining cell type information c_n and random vector u_n, we create a new low-dimensional vector

$$z_n \sim \mathcal{N}(f_z^\mu(u_n, c_n), f_z^\sigma(u_n, c_n))$$

where f_z^μ and f_z^σ are two functions parametrized by neural networks. Given $l_\mu \in \mathbb{R}_+^K$ and $l_\sigma \in \mathbb{R}_+^K$ specified per dataset as in [29], latent variable

$$l_n \sim \text{LogNormal}(l_\mu, l_\sigma^2)$$

encodes a cell-specific scaling factor. Let $\theta \in \mathbb{R}_+^G$ encode a gene specific inverse dispersion parameter (inferred as in [29]). Given the dataset information s_n, conditional distribution $x_{ng} \mid z_n, l_n, c_n$ is conform to the one from the scVI model

$$w_{ng} \sim \text{Gamma}(f_w^g(z_n, \gamma_n), \theta_g)$$
$$y_{ng} \sim \text{Poisson}(l_n w_{ng})$$
$$h_{ng} \sim \text{Bernoulli}(f_h^g(z_n, \gamma_n))$$
$$x_{ng} = \begin{cases} y_{ng} & \text{if } h_{ng} = 0, \\ 0 & \text{otherwise.} \end{cases}$$

where f_w and f_h are functions parametrized by neural networks. f_w has a final softmax layer to represent normalized expected frequencies of gene expression as in [29]. In this model, annotation c_n can be either observed or unobserved following [31, 65], which is useful in our applications where some datasets would come partially labeled or unlabeled. Only the first part of the generative model, as separated above, differs from the original scVI formulation. This corresponds to the top part of the new representation of the graphical model in **Figure 1d**.

Posterior inference

As in [29], we integrate the random variables $\{w_{ng}, y_{ng}, h_{ng}\}$ to simplify our model ($x_{ng} \mid z_n, l_n, s_n$ is zero-inflated negative binomial). We use variational inference, neural networks and the stochastic gradients variational Bayes estimator [30] to perform efficient approximate inference over the latent variable $\{z_n, u_n, c_n, l_n\}$. We assume our variational distribution factorizes as

$$q_\Phi(c_n, z_n, l_n, u_n \mid x_n, s_n) = q_\Phi(z_n \mid x_n) q_\Phi(c_n \mid z_n) q_\Phi(l_n \mid x_n) q_\Phi(u_n \mid c_n, z_n)$$

Following [31, 65], we derive two variational lower bounds: one $\mathcal{L}$ in the case of c_n observed for $p_\Theta(x_n, c_n \mid s_n)$ and a second $\mathcal{U}$ in the case of c_n non-observed for $p_\Theta(x_n \mid s_n)$ where Θ are

all the parameters (neural networks and inverse-dispersion parameters). Equations to derive the *evidence lower bound* (ELBO) are derived in **Supplementary Note 2**. We optimize the sum ELBO $= \mathcal{L} + \mathcal{U}$ over the neural networks parameters and the inverse-dispersion parameters (in a variational Bayesian inference fashion). We discuss the possible ways to train this composite ELBO are referenced in **Supplementary Note 3**. Remarkably, the approximate posterior $q_\Phi(c_n \mid z_n)$ can be used as a classifier, assigning cells to cell types based on the location on the latent space.

We sample from the variational posterior using the reparametrization trick [30] as well as "mini-batches" from the dataset to compute unbiased estimate of the objective gradients' with respect to the parameters. We use Adam [66] as a first-order stochastic optimizer to update the model parameters.

Hyperparameters

For all harmonization tasks in this paper, we consistently use the same set of hyperparameters. Each network has exactly 2 fully-connected layers, with 128 nodes each. The number of latent dimensions is 10, the same as other algorithms for benchmarking purposes (e.g., the number of canonical correlation vectors used in Seurat Alignment). The activation functions between two hidden layers are all ReLU. We use a standard link function to parametrize the distribution parameters (exponential, logarithmic or softmax). Weights for the first hidden layer are shared between f_w and f_h. We use Adam with $\eta = 0.001$ and $\epsilon = 0.01$. We use deterministic warmup [67] and batch normalization [68] in order to learn an expressive model. When we train scANVI, we therefore assume that the data comes from a set of $C_{observed} + C_{unobserved}$ populations, each generated by a different distribution of z_n values. This set includes the $C_{observed}$ populations for which annotated cells are available, and $C_{unobserved}$ population that accounts for cell types for which an annotation is not available to the algorithm. Ad-hoc training procedures for scANVI inference are described in **Supplementary Note 3**. In the case of a one single dataset, we use a 2 fully-connected layers with 256 hidden units classifier with $c = 1$ epochs of classifier training in between each variational update. In the case of transfer of labels, we use **Algorithm 2** with 1 fully-connected layers with 128 hidden units classifier, with $c = 100$ epochs of classifier training in between each variational update.

Bayesian differential expression

scVI For each gene g and pair of cells (z_a, z_b) with observed gene expression (x_a, x_b) and dataset identifier (s_a, s_b), we can formulate two mutually exclusive hypotheses:

$$\mathcal{H}_1^g := \mathbb{E}_s f_w^g(z_a, s) > \mathbb{E}_s f_w^g(z_b, s) \quad \text{vs.} \quad \mathcal{H}_2^g := \mathbb{E}_s f_w^g(z_a, s) \leq \mathbb{E}_s f_w^g(z_b, s),$$

where the expectation $\mathbb{E}_s$ is taken with the empirical frequencies. Notably, we propose a hypothesis testing that do not calibrate the data to one batch but will find genes that are consistently differentially expressed. Evaluating which hypothesis is more probable amounts to evaluating a Bayes factor [69] (Bayesian generalization of the p-value) which is expressed as

$$K = \log_e \frac{p(\mathcal{H}_1^g \mid x_a, x_b)}{p(\mathcal{H}_2^g \mid x_a, x_b)}.$$

The sign of K indicates which of $\mathcal{H}_1^g$ and $\mathcal{H}_2^g$ is more likely. Its magnitude is a significance level and throughout the paper, we consider a Bayes factor as strong evidence in favor of a hypothesis if $|K| > 3$ [70] (equivalent to an odds ratio of $exp(3) \approx 20$). Notably, each of the probabilities in the likelihood ratio for K can be approximated via the variational distribution

$$p(\mathcal{H}_1^g \mid x_a, x_b) \approx \sum_s \iint_{z_a, z_b} p(f_w^g(z_a, s) \leq f_w^g(z_b, s)) p(s) dq(z_a \mid x_a) dq(z_b \mid x_b),$$

where $p(s)$ designated the relative abundance of cells in batch s and all of the measures are low-dimensional, so we can use naive Monte Carlo to compute these integrals. We can then use a Bayes factor for the test.

Since we assume that the cells are independently distributed, we can average the Bayes factors across a large set of randomly sampled cell pairs, one from each subpopulation. The average factor will provide an estimate of whether cells from one subpopulation tend to express g at a higher frequency.

scANVI In the case of scANVI, we need not rely on specific cells since labels are given during the training. We still use a generative model but with the following probability for $p(\mathcal{H}_1^g \mid c_a, c_b)$ where c_a (resp. c_b) is the first (resp. second) cell type of interest,

$$p(\mathcal{H}_1^g \mid c_a, c_b) \approx \sum_s \iint_{u_a, u_b, z_a, z_b} p(f_w^g(z_a, s) \le f_w^g(z_b, s)) p(s) dq(z_a \mid u_a, c_a) dq(z_b \mid u_b, c_b) dp(u_a) dp(u_b).$$

Scalability From a scalability perspective, our methods scales to a million cells in less than an our as reported in our original manuscript [29]. Remarkably, our inference procedure is scalable with respect to the number of batches (with number of floating point operations linear per dataset per iterations) while even the most efficiently implemented method such as Scanorama needs to compare each dataset pairs (quadratic). Our runtime on the large dataset from Scanorama is 42 min for 250 iterations over 100K cells from 26 datasets, still 30 min longer than their algorithm. We expect that further work on implementation details such as GPU usage efficiency, memory loading, data format and iteration monitoring will help close the computational gap between these algorithms.

Gene Selection A common practice in data harmonization is to perform gene selection prior to harmonization. This assumption is critical when the number of genes that can be taken into account by the algorithm is small and potentially biological signal could be lost. scVI is however designed for large datasets which do not fall into the high-dimensional statistics data regime. Remarkably, there is no need for crude gene filtering as part of our pipeline and we adopt it as part of this publication only for concerns of fairness in benchmarking.

Datasets

We report an extensive list of datasets at **Supplementary Table 1**. For all UMI based datasets we took the raw counts without any normalization as input to scVI. For real datasets, we calculated the dispersion (variance to mean ratio) for all genes using Seurat in each dataset and selected $g = 1,000$ genes with the highest dispersion from each. The performance of scVI is not as affected by gene set and we use the same gene selection scheme as in [13] to ensure fairness in our comparison. We then took the union of these gene list as input to Seurat Alignment, MNN and scANVI. One exception is the differential expression study for which we kept the gene set ($g = 3,346$) to have it match the bulk reference as in [29].

Normalization of SmartSeq2 data For the MarrowMT-ss2 dataset, we normalized the read counts per gene by relative transcript length (average transcript lengths of a gene divided by average gene length over all genes), and subsequently took the integer part of the normalized count. This is different from standard normalization procedures in that we do not normalize by cell size because cell size normalization can be performed by scVI. And we only keep the integer part of the counts, due to the distributional assumptions made by scVI. The scVI model can to be extended to fit data with amplification bias, however we have not done so for this paper and thus have to perform this normalization heuristic.

Normalization of CITE-seq data Since we did not explicitly model the CITE-seq data in our models, we normalized it by fitting a Gaussian mixture model to each individual protein with two components. We then transformed each individual protein count as $x \mapsto (x - \frac{\mu_1 + \mu_2}{2})_+$ where μ_1 and μ_2 designate the mean of the mixtures and $._+$ is the positive part of a real number.

Algorithms for benchmarking

Seurat Alignment We applied the Seurat Alignment procedure from the R package Seurat V2.3.3. The number of canonical correlation vectors is 10 for all the datasets, which is also identical to the number of latent dimensions used for scVI and scANVI.

Seurat PCA   We applied the Seurat PCA procedure from the R package Seurat V2.3.3. This method is a simple PCA based after normalization by Seurat. Seurat PCA is used to obtain the individual dataset latent space to evaluate the k-nearest neighbors purity for all non-scVI based methods. The number of principal components is 10.

Matching Mutual Nearest Neighbors   We used the mnnCorrect function from https://rdrr.io/bioc/scran/man/mnnCorrect.html with default parameters.

scmap   We applied the scmap-cluster procedure from the R package scmap. As the scmap manuscript insists heavily on why the M3Drop [71] gene filtering procedure is crucial to overcome batch effects and yield accurate mapping, we let scmap choose its default number of genes ($g = 500$) with this method.

ComBat   We used the R package sva with default parameters.

UMAP   We used the umap class from the UMAP package with a default parameters and spread=2.

DBSCAN   We used the DBSCAN algorithm from the Python package from the python package scikit-learn V0.19.1 and we searched for an optimal hyperparameter combination by a grid search over `eps` and `min_samples` from the range of $0.1 - 2$ and $5 - 100$ respectively. Although some combinations of parameters yield more than one clusters, the smaller clusters comprise of less than 1% of the data. We then evaluated DBSCAN with `eps=1.23, min\_samples=10` and default values for all other hyper-parameters.

PhenoGraph   We used the phenograph.cluster function from the Python package PhenoGraph 1.5.2 downloaded from https://github.com/jacoblevine/PhenoGraph with its default parameters.

Evaluations metrics

Batch Entropy Mixing   Fix a similarity matrix for the cells and take U to be a uniform random variable on the population of cells. Take B_U the empirical frequencies for the 50 nearest neighbors of cell U being a in batch b. Report the entropy of this categorical variable and average over $T = 100$ values of U.

k-nearest neighbors purity   Compute two similarity matrices for cells from the first batch, one from the latent space obtained with only cells from the first batch and the other from the latent space obtained using both batches of cells. We always rely on the euclidean distance on the latent space. Take the average ratio of the intersection of the k-nearest neighbors graph from each similarity matrix over their union. Compute the same statistic for cells from the other batch and report the average of the two.

Weighted and unweighted accuracy   We can evaluate accuracy of cell type classification by comparing prediction to the previously published labels. The unweighted accuracy is the percentage of cells that have the correct label. The weighted accuracy is when the accuracy is calculated for each cell type first and averaged across cell types. The weighted accuracy assigns the same weight to each cell type and thus weighs correct prediction of rare cell types more heavily than the unweighted accuracy. All accuracies reported in this paper is the weighted accuracy.

Maximum Posterior Probability   We evaluate the performance of the scANVI classifier at transferring labels from an annotated dataset to an unannotated dataset by looking at the maximum posterior probability for the observed classes. By default scANVI classifier sets the number of classes to the same number of cell types in the merged dataset. In the case of N observed labels from the annotated dataset and one unannotated dataset (thus the cell type label is "Unlabeled") scANVI assumes $N + 1$ classes. For each cell, scANVI assigns a posterior

probability for each of the $N+1$ classes. The maximum posterior probability for the observed classes is the highest probability of a cell being assigned to one of the N observed classes.

Signature for sub-division of T cells in human PBMCs

Gene sets For ranking the cells, we used both positive and negative sets of genes:

- **CD4 Regulatory**: *GITR+ CTLA4+ FOXP3+ CD25+ S100A4- CD45- CD8B-*

- **CD4 Naive**: *CCR7+ CD4+ S100A4- CD45- FOXP3- IL2RA- CD69-*

- **CD4 Memory**: *S100A4+ CD25- FOXP3- GITR- CCR7-*

- **CD8 Naive**: *CD8B+ CCR7+ CD4-*

Signature calculus To compute the signature of a cell, we followed the normalization procedure from [24] which consists in dividing by total numbers of UMIs, applying a entry-wise transformation $x \mapsto \log(1 + 10^4 x)$ and z-score normalization for each gene. Then, we aggregated over the genes of interest for each cell by applying the sign from the gene-set and averaging.

Software Availability

An open-source software implementation of scVI is available on Github (https://github.com/YosefLab/scVI). All code for reproducing results and figures in this manuscript is deposited at https://doi.org/10.5281/zenodo.2529945.

Data availability

All of the datasets analyzed in this manuscript are public and referenced at https://github.com/chenlingantelope/HarmonizationSCANVI.

Supplementary Figures
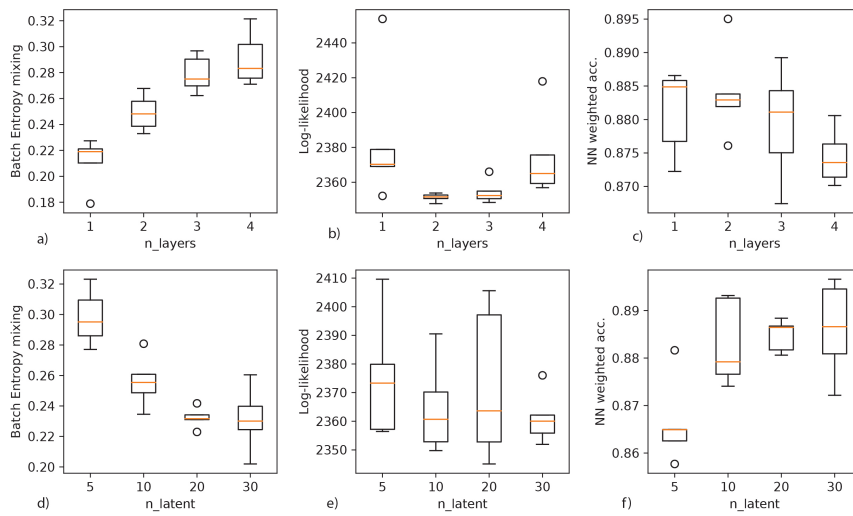
Figure 1: Robustness analysis for harmonization of the pair of datasets MarrowMT-10x / MarrowMT-ss2 with scVI. $(a-c)$ We augment the number of hidden layers in the neural network f_w and track across $n = 5$ random initializations for the batch entropy mixing (a), the held-out log likelihood (b) and the weighted accuracy of a neares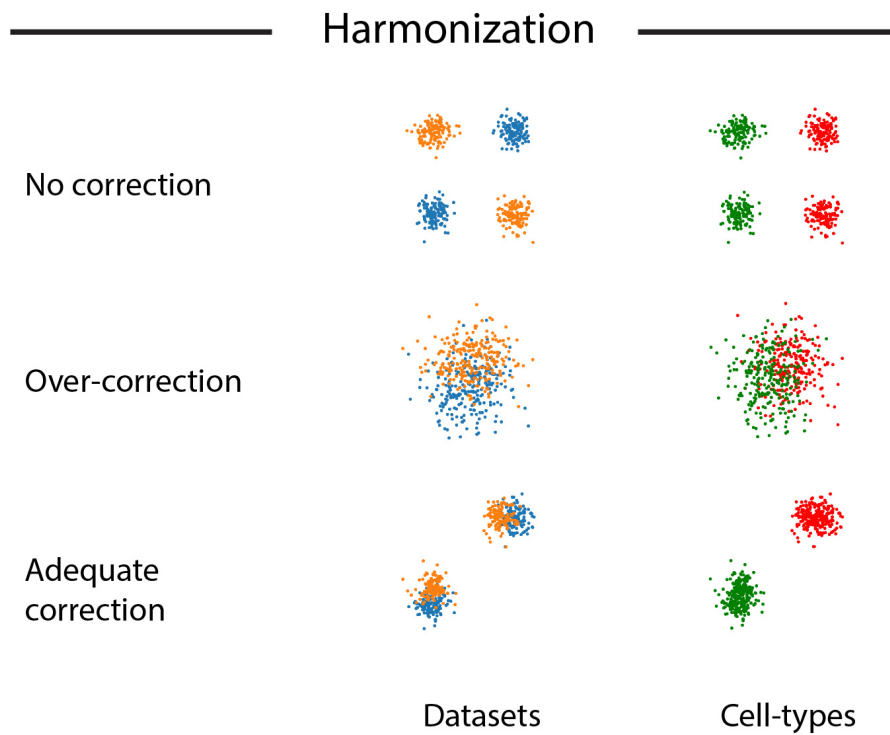t neighbor classifier on the latent space (c). $(d-f)$ We increase the number of dimensions for the latent variable z and track across $n = 5$ random initialization the batch entropy mixing (d), the held-out log likelihood (e) and the weighted accuracy of a nearest neighbor classifier on the latent space (f)

Figure 2: Schematic of the data harmonization problem. We are provided with two datasets (orange and blue), each consisting of two cell types (red and green). Our evaluation for the harmonization problem consists of two objectives: (1) mixing the two datasets well and (2) retaining the original structure in each dataset. Scenario 1 (top) is the case of under correction where objective (2) is achieved while objective (1) is not. Scenario 2 (middle) is the case of over correction where objective (1) is improved while objective (2) becomes worse. The bottom panel shows the desired scenario of mixing the datasets well while retaining the biological signal.
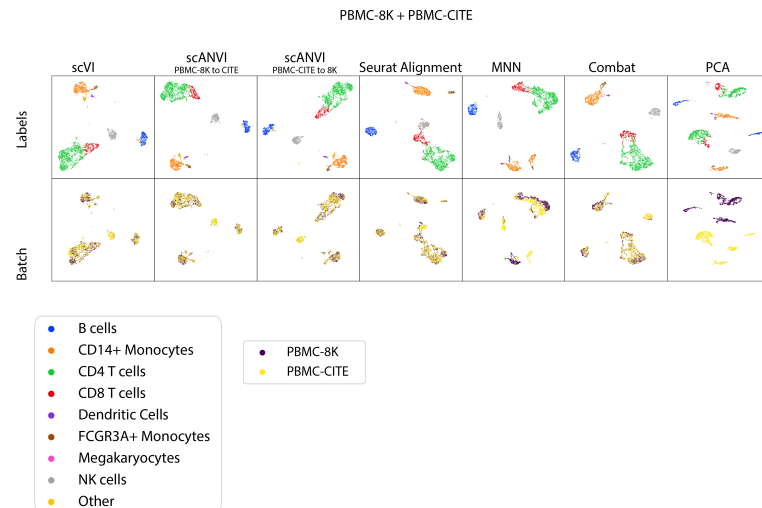
Figure 3: Visualization of the benchmark PBMC-8K / PBMC-CITE. all positions for the scatter plots are derived using UMAP on the latent space of interest.
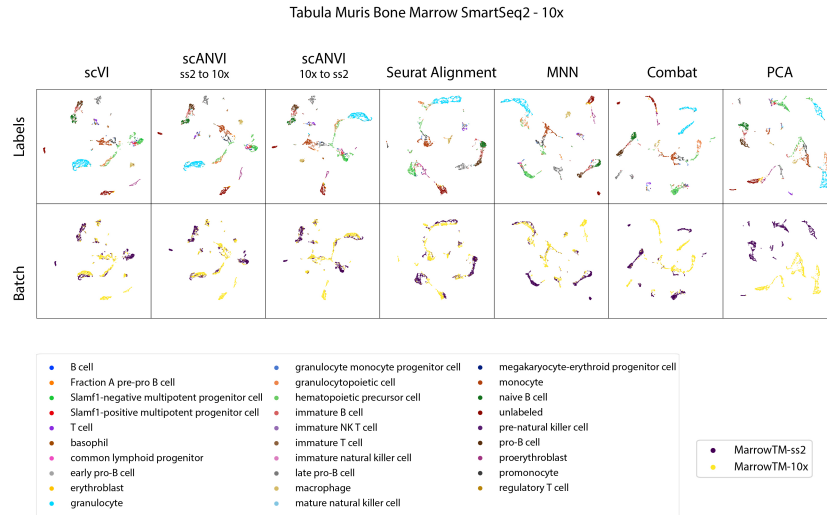
Figure 4: Visualization of the benchmark MarrowMT 10x / ss2. all positions for the scatter plots are derived using UMAP on the latent space of interest.
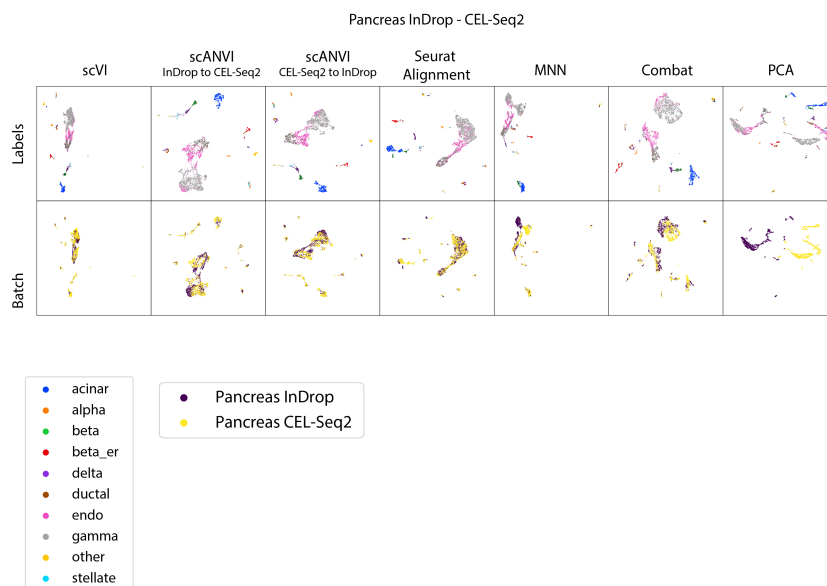

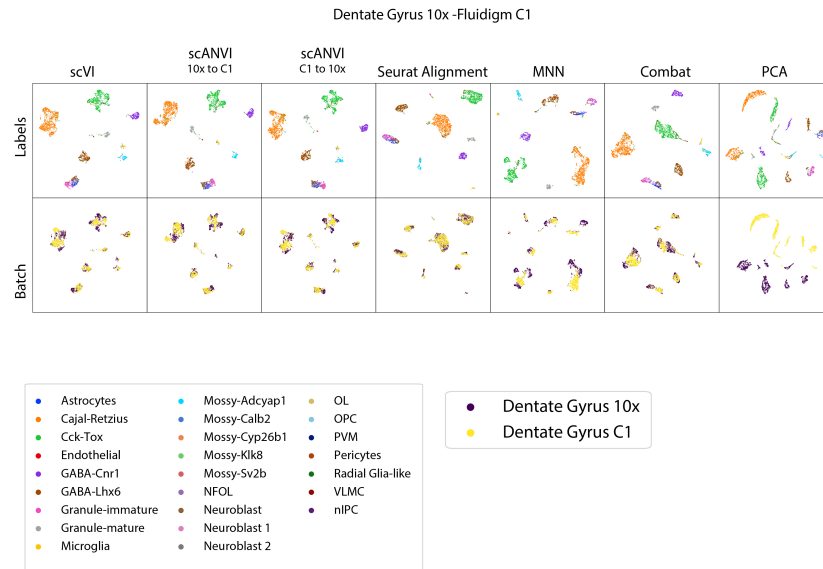Figure 5: Visualization of the benchmark Pancreas InDrop / CEL-Seq2. all positions for the scatter plots are derived using UMAP on the latent space of interest.

Figure 6: Visualization of the benchmark Dentate Gyrus 10X - Fluidigm C1. all positions for the scatter plots are derived using UMAP on the latent space of interest.
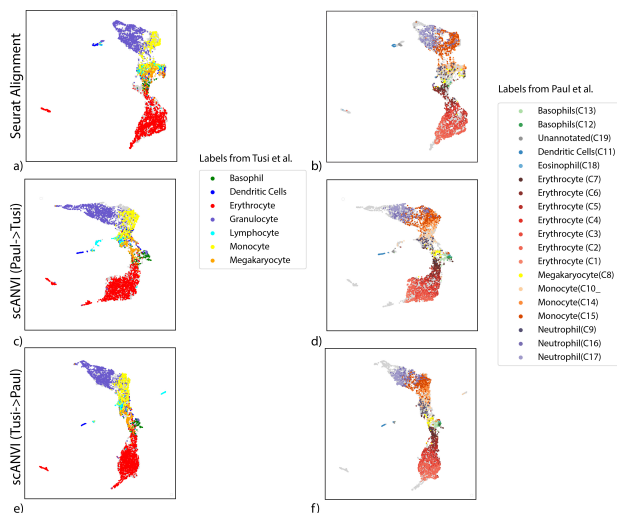

Figure 7: $(a - b)$ Continuous trajectory obtained by the Seurat Alignment procedure for the HEMATO-Tusi and the HEMATO-Paul datasets. $(c - d)$ Continuous trajectory obtained by the scANVI using the Tusi cell type labels for semi-supervision. $(e - f)$ Continuous trajectory obtained by the scANVI using the Paul cluster labels for semi-supervision. All locations for scatter plots are computed via UMAP in their respective latent space.
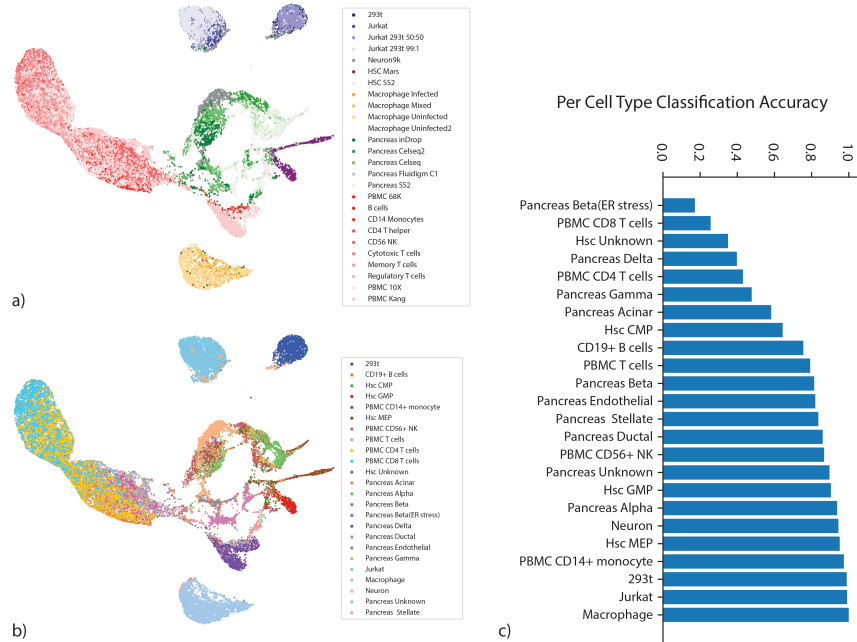
Figure 8: Large Scale data integration with scVI. $(a - b)$ UMAP visualization of the scVI latent space colored by datasets (a) and by cell types (b). (c) accuracy of a nearest neighbor classifier based on scVI latent space
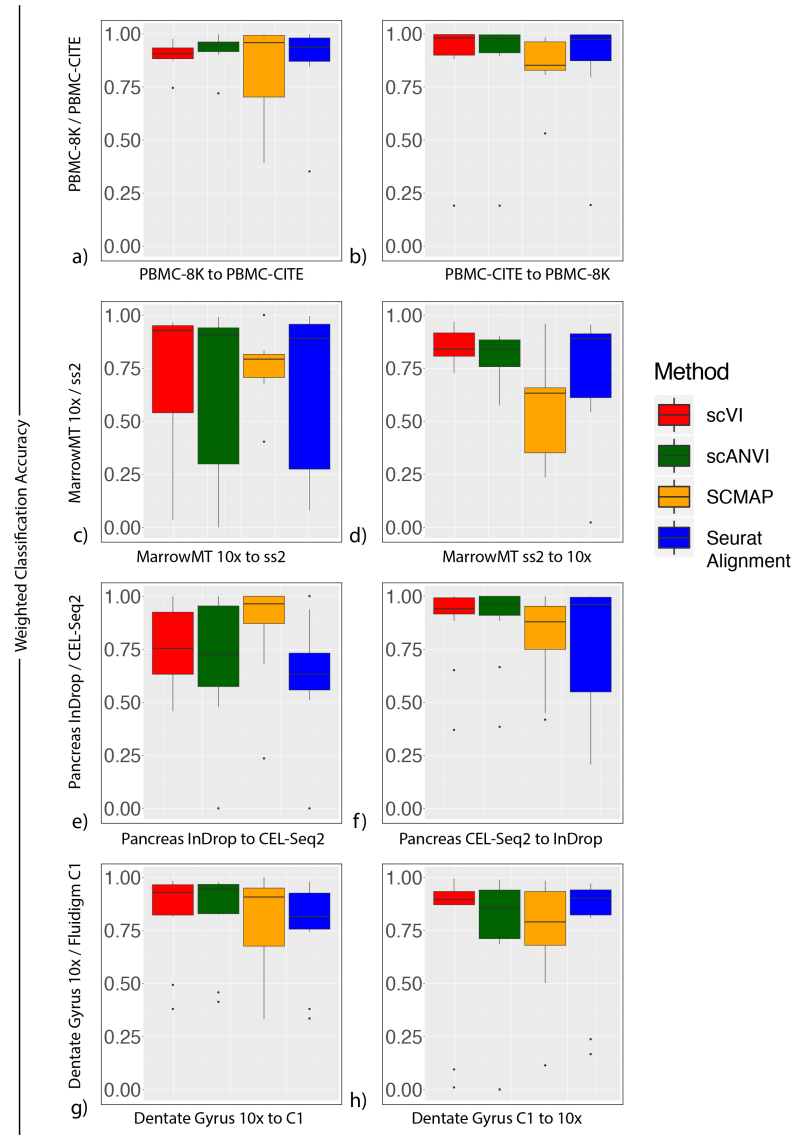
Figure 9: Annotation results for the PBMC-8K / PBMC-CITE $(a - b)$, the MarrowMT-10X / MarrowMT-SS2 datasets datasets $(c - d)$, Pancreas InDrop-CITESeq $(e - f)$ and Dentate Gyrus 10X / Fluidigm C1 $(g - h)$. Accuracies for transferring annotations from one dataset to another from a k-nearest neighbor classifier on Seurat Alignment, k-nearest neighbor classifier on scVI latent space, scANVI classifier and SCMAP classifier are shown. The aggregated results across for cell types that are shared between the two datasets is shown in box plots.
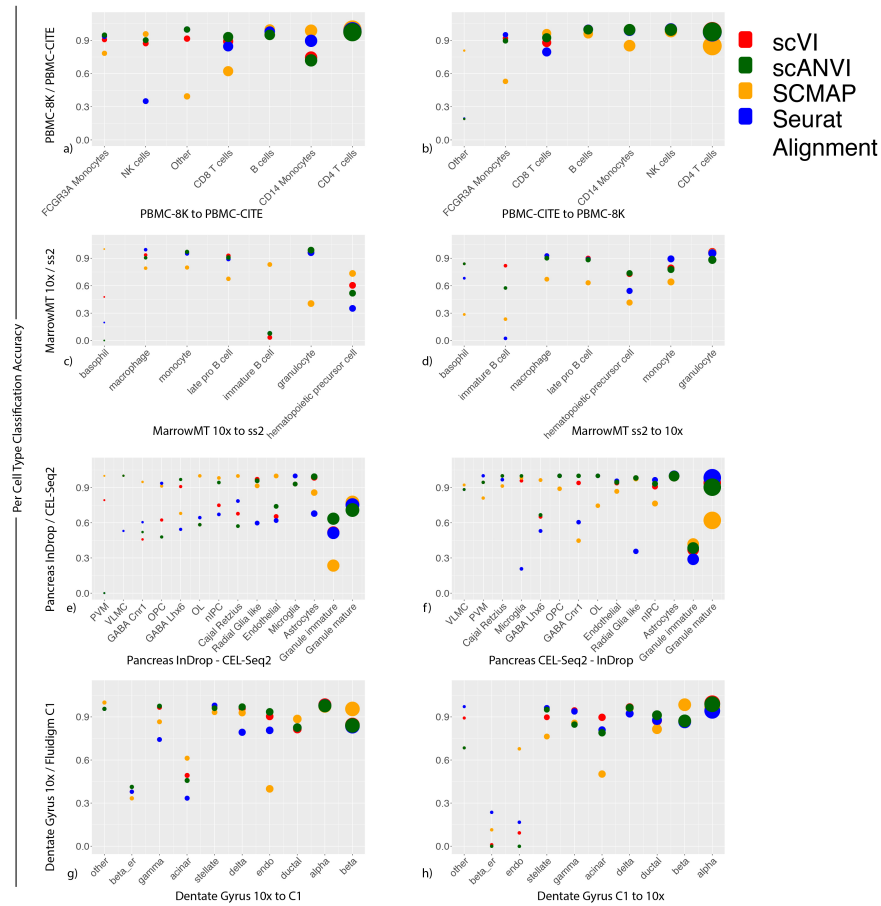
Figure 10: Annotation results for the PBMC-8K / PBMC-CITE $(a-b)$, the MarrowMT-10X / MarrowMT-SS2 datasets datasets $(c-d)$, Pancreas InDrop-CITESeq $(e-f)$ and Dentate Gyrus 10X / Fluidigm C1 $(g-h)$. Accuracies for transferring annotations from one dataset to another from a k-nearest neighbors classifier on Seurat Alignment, k-nearest neighbors classifier on scVI latent space, scANVI classifier and SCMAP classifier are shown. The prediction accuracy for each cell type that is shared between the two datasets is shown on the y-axis and the size of the dots are proportional to the proportion of a cell type in the total population.
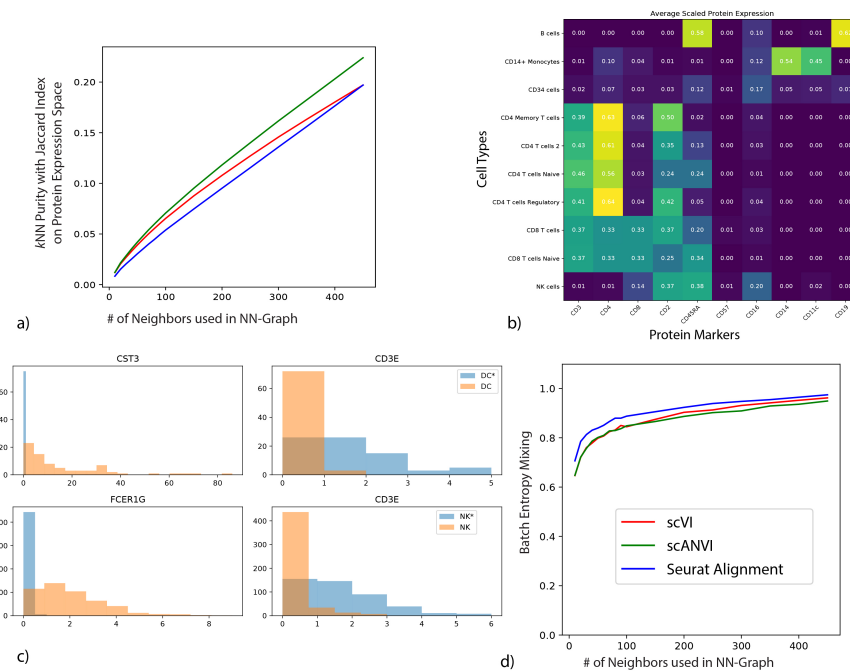
Figure 11: (a) k-nearest neighbors purity of the merged latent space on the protein expression space as a function of the size of the neighborhood. (b) Protein expression heatmap showing consistency of PBMC-sorted labels and protein expression in PBMC-CITE. The protein expression per cell type is based on k-nearest neighbors imputation from the harmonized latent space obtained from scANVI trained with pure population labels. (c) We select individual cells that were labeled as Dendritic cells or Natural Killer cells in the original publication of the respective datasets, and compare the raw transcript count from cells inside the scANVI T cells cluster (DC*, NK*) against cells outside the T cells cluster (DC, NK). The expression of marker genes suggest that DC* and NK* is more likely to be T cells and thus the scANVI latent space is more accurate. (d) The batch entropy mixing of the three datasets in scVI, scANVI and Seurat Alignment merged space.
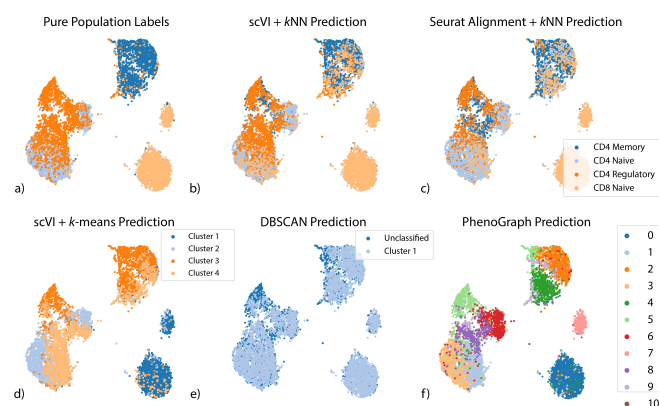

Figure 12: Other methods of classifying T-cell subsets of the PBMC-Pure dataset. Coordinates for the scatter plots are derived from UMAP embedding based on the latent space of scANVI. (a) Ground truth labels from the purified PBMC populations (b) k-nearest neighbors classification labels when applied on scVI latent space from the seed set of cells (c) k-nearest neighbors classification labels when applied on Seurat Alignment latent space (d) k-means clustering based labels when applied to scVI latent space (e) DBSCAN clustering based labels when applied to scVI latent space. DBSCAN returns only one cluster but return some cells as unclassified. (f) PhenoGraph clusters on scVI latent space
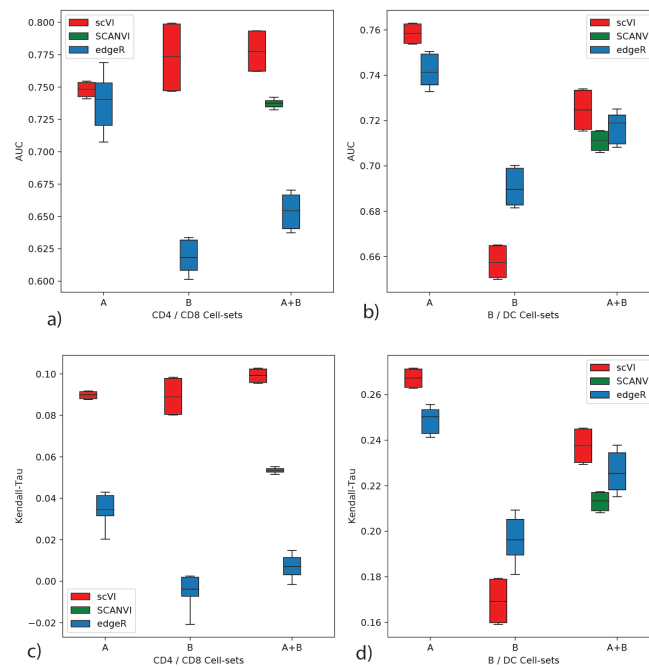
Figure 13: Differential Expression on mulitple datasets with scVI. Evaluation of consistency with the AUROC metric is shown for comparisons of CD4 vs CD8 T cells (a) and B cells vs Dendritic cells (b) on the PBMC-8K only (A), the PBMC-68k only (B) and the merged PBMC-8K / PBMC-68K (A+B) for scVI and edgeR. Error bars are obtained by multiple subsampling of the data to show robustness. ($c - d$) Same plots with the Kendall Tau metric.

Harmonization and Annotation of Single-cell Transcriptomics data with Deep Generative Models

Supplementary Information

Chenling Xu[*1], Romain Lopez[*2], Edouard Mehlman[*2,3],
Jeffrey Regier[2], Michael I. Jordan[2,4] & Nir Yosef[†,1,2,5,6]

[1]Center for Computational Biology
University of California, Berkeley

[2]Department of Electrical Engineering and Computer Sciences
University of California, Berkeley

[3]Centre de Mathématiques Appliquées
Ecole polytechnique, Palaiseau

[4]Department of Statistics
University of California, Berkeley

[5]Ragon Institute of MGH, MIT and Harvard

[6]Chan-Zuckerberg Biohub Investigator

[*] These authors contributed equally to this work.

[†] Corresponding author. Email: niryosef@berkeley.edu (N.Y.).

Supplementary Tables

List of Tables

Dataset Name	Tech.	n cells	Description	Ref.
PBMC-8K	10x	8,381	peripheral blood mononuclear cells (PBMCs) from a healthy donors; labels extracted from [72]	[33]
PBMC-CITE	10x	7,667	PBMCs obtained from CITE-seq; labels generated manually by inspection of protein marker level on Seurat clusters	[25]
PBMC-68K	10x	68,579	fresh PBMCs collected from healthy donor	[3]
PBMC-Sorted	10x	94,655	Bead-purified PBMCs collected from the same donor as PBMC68K	[3]
MarrowTM-10x	10x	4,112	Mouse bone marrow cells collected from two female mice	[9]
MarrowTM-ss2	Smart-Seq2	5,351	FACS sorted cells (B cells, T cells, granulocytes and Kit (+), Sca-1 (+) and Lin (-) hematopoietic stem cells) from 3 male and 2 female mice,	[9]
Pancreas-InDrop	inDrop	8,569	Human Pancreas	[40]
Pancreas-CEL-Seq2	CEL-Seq2	2,449	Human Pancreas	[73]
DentateGyrus-10x	10x	5,454	Mouse Dentate Gyrus	[41]
DentateGyrus-C1	Fluidigm C1	2,303	Mouse Dentate Gyrus	[41]
CORTEX	10x	160,796	Mouse Nervous System	[52]
HEMATO-Tusi	inDrop	4,016	Hematopoeitic Progenitor Mouse Cells	[43]
HEMATO-Paul	MARS-seq	2,730	Hematopoeitic Progenitor Mouse Cells	[44]
SCANORAMA	Mixture	105,476	human cells from 26 diverse scRNA-seq experiments across 9 different technologies	[19]

Table 1: List of dataset used in this paper. Note that for the PBMC-Sorted 11 cell types were collected according to the paper but only 10 are available from the 10x website. [33]

cell-type	PBMC-8K proportion	PBMC-CITE proportion
NK cells	0.036	0.178
CD8 T cells	0.119	0.091
B cells	0.133	0.104
FCGR3A+ Monocytes	0.028	0.029
CD14+ Monocytes	0.186	0.159
CD4 T	0.421	0.436
Dendritic Cells	0.026	0
Megakaryocytes	0.008	0
Other	0.043	0.004

Table 2: Compositions of cell-types in the PBMC-8K and the PBMC-CITE dataset

Cell Types	# cells
B cells	10,085
CD14+ Monocytes	2,612
CD34+ cells	9,232
CD4 T cells	11,213
CD56 NK cells	8,385
CD8 T cells	10,209
Memory T cells	10,224
Naive CD8 T cells	11,953
Naive T cells	10,479
Regulatory T cells	10,263

Table 3: Cell types present in the PBMC-sorted dataset.

Supplementary Note 1   Statistical trade-offs in scRNA-seq harmonization

Harmonization is a hard and ill-defined problem. Especially, it can be difficult to formulate exactly its objective and at which level of granularity the "harmonization" is expected. Let us take the example of two PBMCs datasets that are exact biological replicates with same experimental conditions. In that case, the problem is well defined since we have a non-confounder assumption. Removing in a principled way all the variation in the data that corresponds to batches is reasonable. However, let's take a slightly trickier case, one patient and one control dataset. If we look at the exact same metrics for harmonization, the resulting algorithm could discard any interesting biology that happens to the cells that get frozen. There is a confounder and the problem is much more difficult (ill-posed).

Therefore, it is extremely important to state how different models perform harmonization and what are their underlying hypothesis and modeling capabilities. For example, scmap [28] proposes a new gene filtering method to select gene that are claimed to be invariant to batch-effects. However, it is clear that over filtering can lead to ignoring biological information. MNNs [12] on its end assumes that the topology of cell types can be easily resolved by a k-nearest neighbor graph using a $\mathbb{L}^2$ normalization and distance scheme. This allows MNNs [12] and all the neighbor-matching-based approaches [20, 19] to remarkably merge batches with the risk of also merging cell types in the case where they are not detectable with this normalization scheme.

scVI and scANVI perform harmonization by learning a common generative model for a collection of gene expression probability distributions $[p(x \mid z, s)]_{s \in \{1, \cdots, K\}}$ indexed by the dataset-identifier s. The statistical richness of the collection of conditional variables $[p(x \mid z, s)]_{s \in \{1, \cdots, K\}}$ dictates the flexibility of our model towards integrating datasets.

One notable factor that sensibly contributes to harmonization capabilities is the prior for cell-specific scaling factor l_n that is dataset-specific. This helps probabilistically removing library-size caused discrepancies in the measurements and is more principled than normalization of the raw data [74]. Another important parameter is the parametrization of the neural network that maps variables (z, γ) to the expected frequencies $\mathbb{E}[w \mid z, s] = f_w(z, s)$. Since our function f_w is now potentially non-linear, our model can benefit from more flexibility and fit batch-specific effects locally for each cell types or phenotypical condition. Especially, depending on how one designs the neural architecture of f_w, it is possible to more flexibly correct dataset-specific effects. More specifically, we treat f_w as a feed-forward neural network for which at each layer we concatenate the batch-identifier with the hidden activations. A consequence of this design is that with more hidden layers in f_w, less parameters are shared and the family of distributions $[p(x \mid z, s)]_{s \in \{1, \cdots, K\}}$ has more flexibility to fit batch-specific effects (**Supplementary Figure 1a-c**). Conversely, when the latent dimension grows, the generative network has less incentive to use the dataset covariate and might mildly duplicate the information in its latent space (**Supplementary Figure 1d-f**). Throughout the paper, we fix those parameters (**Online Methods** and show competitive performance for all our datasets.

Another insight comes from how the variational distribution $q(z \mid x, s)$ is parametrized. Our neural networks plays the role of an explicit stochastic mapping from the gene expression x_n of a single-cell n to a location in a latent space z_n (a standard theme in scRNA-seq analysis, e.g LIGER [18], Seurat [13], scVI [29]). Via this map, we match an empirical distribution in gene expression space (i.e a dataset) $p_{\text{data}}(x, s) = \sum_n \delta_{(x_n, s_n)}(x, s)$, with a certain distribution on the latent space $p_{\text{data}}(z) = \sum_n \delta_{\Phi(x_n, s_n)}(z)$. In certain cases, even though we designed this latent space to represent biological signal, the transformed dataset might still be confounded by technical effects [75]. In particular, this effect is susceptible to be severe when the generative model is not flexible enough to fit the dataset-specific effects or has a model misfit (as in, to some extent, the case with the CCA of [13] that assumes the data is log-normal). In this case, the go-to method is to empirically constrain the mapping (i.e the variational network in our case or the latent space itself in the case of SEURAT) to match the collections of variables $p_{\text{data}}(z, s)_{s \in \{1, \cdots, K\}}$. However, each of these correction approaches has underlying modeling assumptions. For example, SAUCIE [21] and MMD ResNet [22] both propose to correct the variational distribution by adding on their objective function a non-parametric measure of distance between distributions (maximum mean discrepancy [76]). This approach specifically assumes that each dataset has the same cell type composition and the same biological signal and which is not reasonable in other cases than biological replicates. Seurat Alignment [13] on its end relies on a milder assumption

that there is a common signal exactly reproducible between the two datasets and that CCA capture most of the biological variation, which is not obvious true considering limited suitability of linear Gaussian model for scRNA-seq. Seurat anchors [20] relies on CCA and suffer from the same problems as MNNs with its specific normalization scheme. Finally, the recent LIGER [18] method at first sight seems like a non-probabilistic version of scVI since it also learns a degenerate conditional distribution via its integrative non-negative matrix factorization [18] (NMF is a noisy-less version of a Gamma-Poisson generative model). However, it has a further quantile normalization of the latent spaces within clusters. First, the output of the clustering algorithm is not necessarily correct and could perturb downstream analyses. Second, if a cell type would be slightly different from one condition to another, this information would be lost in the final latent space. Overall, all these correction methods can therefore potentially lead to over-correction and statistical artifacts [32].

Supplementary Note 2   Evidence Lower Bound decomposition

For notational convenience, we do not write here that all the probabilities are conditioned on the batch identifier s. We also report the evidence lower bound (ELBO) only for one sample (i.e one cell) and drop the index notations by substituting $\{x_n, z_n, u_n, c_n, l_n\}$ by $\{x, z, u, c, l\}$. This is without loss of generality since all the cells are independent and identically distributed under our model. Bayesian inference aims at maximizing the marginal likelihood of our datapoints. We also drop the parameters Θ (resp. Φ) of the generative model (resp. the variational distribution) for notational convenience. We will derive the ELBO in the case where c is not observed (almost same calculations resolve the case where c is observed). Notably, we derive the ELBO using Jensen inequality weighted by the variational distribution $q(z, u, l, c \mid x)$. Similar derivations can be found in the variational autoencoder literature (eg. [65]). We assume our variational distribution factorizes as:

$$q(c, z, u, l \mid x) = q(z \mid x)q(c \mid z)q(u \mid z, c)q(l \mid x)$$

$$
\begin{aligned}
\log p(x) \geq & \mathbb{E}_{q(z,u,c,l \mid x)}\left[\log \frac{p(x,z,u,c,l)}{q(z,u,c,l \mid x)}\right] = \mathbb{E}_{q(z,u,c,l \mid x)}\left[\log \frac{p(x \mid z,l)p(z \mid u,c)p(c)p(u)p(l)}{q(z,u,c,l \mid x)}\right] \\
\geq & \underbrace{\mathbb{E}_{q(z,u,c,l \mid x)}\left[\log p(x \mid z,l)\right]}_{(i)} + \underbrace{\mathbb{E}_{q(z,u,c,l \mid x)}\left[\log \frac{p(z \mid u,c)}{q(z \mid x)}\right]}_{(ii)} \\
& + \underbrace{\mathbb{E}_{q(z,u,c,l \mid x)}\left[\log \frac{p(c)}{q(c \mid z)}\right]}_{(iii)} + \underbrace{\mathbb{E}_{q(z,u,c,l \mid x)}\left[\log \frac{p(u)}{q(u \mid z,c)}\right]}_{(iv)} \\
& + \underbrace{\mathbb{E}_{q(z,u,c,l \mid x)}\left[\log \frac{p(l)}{q(l \mid x)}\right]}_{(v)}
\end{aligned}
\tag{1}
$$

Then we simplify each individual term of the ELBO in 1 by recognizing KL divergence terms. In particular, we use subscript notation $\mathbb{KL}_{\mathrm{G}}\left(.||.\right)$, and $\mathbb{KL}_{\mathrm{M}}\left(.||.\right)$ to denote Gaussian and multinomial KL divergences.

$$\mathbb{E}_{q(z,u,c,l \mid x)}\left[\log p(x \mid z,l)\right] = \mathbb{E}_{q(z \mid x)q(l \mid x)}\left[\log p(x \mid z,l)\right] \tag{i}$$

$$\mathbb{E}_{q(z,u,c,l \mid x)}\left[\log \frac{p(z \mid u,c)}{q(z \mid x)}\right] = \mathbb{E}_{q(z \mid x)}\left[\mathbb{E}_{q(u \mid z,c)q(c \mid z)}\left[\log \frac{p(z \mid u,c)}{q(z \mid x)}\right]\right] \tag{ii}$$

$$= \mathbb{E}_{q(z \mid x)}\left[\sum_{c=1}^{K} q(c \mid z)\mathbb{E}_{q(u \mid z,c)}\left[\log \frac{p(z \mid u,c)}{q(z \mid x)}\right]\right]$$

$$\mathbb{E}_{q(z,u,c,l \mid x)}\left[\log \frac{p(c)}{q(c \mid z)}\right] = \mathbb{E}_{q(z \mid x)}\left[\underbrace{\sum_{c=1}^{K} q(c \mid z)\log \frac{p(c)}{q(c \mid z)}}_{-\mathbb{KL}_{\mathrm{M}}(q(c \mid z)||p(c))}\right] \tag{iii}$$

$$\mathbb{E}_{q(z,u,c,l \mid x)}\left[\log \frac{p(u)}{q(u \mid z,c)}\right] = \mathbb{E}_{q(z \mid x)}\left[\sum_{c=1}^{K} q(c \mid z)\underbrace{\mathbb{E}_{q(u \mid z,c)}\left[\log \frac{p(u)}{q(u \mid z,c)}\right]}_{-\mathbb{KL}_{\mathrm{G}}(q(u \mid z,c)||p(u))}\right] \tag{iv}$$

$$\mathbb{E}_{q(z,u,c,l \mid x)}\left[\log \frac{p(l)}{q(l \mid x)}\right] = -\mathbb{KL}_{\mathrm{G}}\left(q(l \mid x)||p(l)\right) \tag{v}$$

Supplementary Note 3   Training Information

In order to train scanVI properly, several options are possible to train all the parameters (θ from the generative model, ϕ from the variational distribution and $\theta^{\mathcal{C}}$ from the labels' posterior exclusively). In all cases, parameters θ and ϕ should minimize the evidence lower bound $\mathcal{J} = \mathcal{L} + \mathcal{U}$ (decomposed over the labeled samples $\mathcal{L}$ and unlabeled samples $\mathcal{U}$). Furthermore, [65] suggests to optimize jointly a modified objective that penalize the ELBO by a classification loss C on the labeled data so that the parameters $\theta^{\mathcal{C}}$ also benefits from the learned data. In [77], we interpreted this extension of the ELBO as a correction term for noisy labels. In this manuscript, we propose a specific training procedure for scANVI, based on alternating minimization on the parameters (θ, ϕ) and $\theta^{\mathcal{C}}$. A joint training, conform to the one suggested in [65] is described in **Algorithm 1**. Instead, an alternate training procedure would perform alternating minimization as described in **Algorithm 2**. The advantage of joint training is presumably that it shapes the latent space directly, through the modification of the encoder's weights. The advantage of the alternate training, is that the learning of the cell type edge converges properly at the end of each epoch, and improve indirectly the latent space quality, through the next steps of optimization. We have noticed in practice that using the joint training in the case of transferring labels from one dataset to another might break down the mixing in the latent space, as the loss C has only contributions from a unique dataset. Therefore, throughout the paper, we consistently used the alternating procedure of **Algorithm 2**.

define $\mathcal{J}_\alpha = \mathcal{J} + \alpha \times C$
repeat
   $(g_\theta, g_\phi) \leftarrow (\frac{\partial \mathcal{J}_\alpha}{\partial \phi}, \frac{\partial \mathcal{J}_\alpha}{\partial \phi})$
   $(\theta, \phi) \leftarrow (\theta, \phi) + \Gamma(g_\theta, g_\phi)$
until $\mathcal{J}_\alpha$ has converged (n epochs)

Algorithm 1: Train jointly

repeat
  repeat
    $(g_\theta, g_\phi) \leftarrow (\frac{\partial \mathcal{J}}{\partial \phi}, \frac{\partial \mathcal{J}}{\partial \phi})$
    $(\theta, \phi) \leftarrow (\theta, \phi) + \Gamma(g_\theta, g_\phi)$
  until $\mathcal{J}$ has converged (1 epochs)
  repeat
    $\theta^{\mathcal{C}} \leftarrow \theta^{\mathcal{C}} + \frac{\partial \mathcal{C}}{\partial \theta^{\mathcal{C}}}$
  until $\mathcal{C}$ has converged (c epochs)
until $\mathcal{J}$ and $\mathcal{C}$ have converged (n epochs)

Algorithm 2: Train alternately (Default scANVI)

Supplementary Note 4 Hierarchical classification

In this note, we explain the modeling details for an extension of scANVI where the cell types annotation can follow a two-level hierarchical structure. Let us note that this can in principle be adapted to any arbitrary tree representation of cell types taxonomy. This taxonomy needs to be hard-coded and known *a priori*.

We do not need to formally modify the graphical model but only how we structure the variable c_n. Notably, we formally pose $c_n = (y_n, y_n^g) \in \{0, \cdots, K\} \times \{0, \cdots, K^g\}$ and consider the original Bayesian network as an hypergraph. In the generative model, the conditional distribution $p(z \mid u, c) = p(z \mid u, y)$. Since the cell type group indicator variable y^g is not as refined than the cell type itself y.

However, what sensibly changes is the parametrization of the variational distribution $q(c \mid z) = q(y, y^g \mid z)$. The prior taxonomy knowledge encapsulates whether the assignment $(y^g, y) = (i, j)$ is biologically possible (i.e cell type i is a sub-population of group cell type j). We encode this biological compatibility into a parent function $\pi : \{0, \cdots, K\} \to \{0, \cdots, K^g\}$ that maps a cell type to its parent in the hierarchy. We note for simplicity $q(y_i, y_j^g \mid z) = q(y = i, y^g = j \mid z)$. We then use two neural networks f and f_g (with softmax non-linearities) that map the latent space to the joint approximate posterior $q(y, y^g \mid z)$ with the following rules:

$$q(y_i, y_j^g \mid z) = \begin{cases} f_i(z) & \text{if } \pi(i) = j, \\ 0 & \text{otherwise.} \end{cases}$$

$$q(y_j^g \mid z) = f_j^g(z)$$

(2)

Then, we can derive the marginal probability over finer cell types classes using the chain rule and Bayes rule:

$$
\begin{aligned}
q(y_i \mid z) &= q(y_i \mid y_{\pi_i}, z) q(y_{\pi_i} \mid z) \\
&= \frac{q(y_i, y_{\pi_i} \mid x)}{q(y_{\pi_j} \mid x)} q(y_{\pi_i} \mid z) \\
&= \frac{q(y_i, y_{\pi_i} \mid x)}{\sum_{j \in c(\pi_i)} q(y_j, y_{\pi_j} \mid x)} q(y_{\pi_i} \mid z) \\
&= \frac{f_i(z)}{\sum_{j \in c(\pi_i)} f_j(z)} f_{\pi_i}^g(z)
\end{aligned}
$$

where $c(\pi_i)$ denotes the set of children of node i children.